Developing a Predictive Model and Novel Imaging Technique for the Failure of Polyethylene Insulators

A Thesis
SUBMITTED TO THE FACULTY OF THE
UNIVERSITY OF MINNESOTA
BY

Daniel Taylor Zoltek

IN PARTIAL FULFILLMENT OF THE REQUIREMENTS
FOR THE DEGREE OF
MASTER OF SCIENCE

Melissa Maurer-Jones, Adviser

August 2019

Acknowledgements

I would like to acknowledge the University of Minnesota Duluth and Department of Energy for funding this project, the University of Minnesota Characterization Facility for help with imaging the gold nanoparticles, and Dr. Zimmer in the medical school for assistance with concentrating the gold nanoparticles.

A special thank you to Dr. Melissa Maurer-Jones and Dr. Brian Hinderliter for being mentors through this project, as well as helping prepare me for my Ph.D. program next year.

To my group members, especially Faith Murphy, Tayler Hebner, Magdalene Jones and Liam Fawcett, for their help both in and outside of lab.

Finally, to my family, the UMD Track and Field team, and especially Maeve Ryan and Alvin Burrows for their help and continuing love and support.

ABSTRACT

Polyethylene is the most widespread polymer used in insulative cable housings due to its low cost, high chemical resistivity and low permeability to liquids and gases. This does not mean, however, that the material is not susceptible to failure under environmental working conditions. Many techniques for monitoring both chemical and physical changes have been developed, though no attempts have been made to integrate these findings. Here, we put forth a model for the failure of polyethylene cable housings under thermooxidative conditions. This model revealed an absence of data on the monitoring of polyethylene crystalline structure during the aging process, which in part controls the insulative properties of the polyethylene. Polyethylene films (30 μm) were aged at 110°C for 24-hour periods in an oven and carbonyl content, a common aging indicator, was monitored. An ATR-FTIR crystallinity monitoring technique was developed and revealed a 3-phase change of crystalline structure upon thermal aging. To better visualize the hypothesized pore formation in the polyethylene, which follows aging, EIS was used to saturate pores with gold nanoparticles before elemental analysis and imaging with SEM. Results suggest the existence of these pores and the ability for ions to penetrate the aged films.

Table of Contents

List of Tables

List of Figures

Chapter 1. Development of a Predictive Aging Model

ABSTRACT

Polyethylene is the most widespread polymer used in insulative cable housings due to its low cost, high chemical resistivity and low permeability to liquids and gases. This does not mean, however, that the material is not susceptible to failure under environmental working conditions. Many techniques for monitoring both chemical and physical changes have been developed, though no attempts have been made to integrate these findings. Here, we put forth a model for the failure of polyethylene cable insulation under thermooxidative conditions. This model revealed an absence of data on the monitoring of polyethylene crystalline structure during the aging process, which in part controls the insulative properties of the polyethylene.

1.1 Introduction

Since the early 1940's, the development of polymers has expanded from household use to materials for industrial infrastructure. The versatility of polymers has arisen from their ability to be easily modified during the polymerization process by introduction of changes to the chemical backbone, leading to increases in strength and flexibility, while decreasing permeability and chemical reactivity. Nylon, for example, has periodic amide groups within hydrocarbon chains which help increase strength and melting point (196℃), but a poor ability to orient into a film structure[1,2]. Polyvinyl chloride exists as a rigid plastic used in piping and can be softened by the introduction of plasticizers but have the potential to leach out[3]. Polyethylene, however, maintains flexibility, easy manufacturing and can be blown into a film extruded into cable insulation of desired thickness. These characteristics have made polyethylene a common choice for use as

insulative barriers in medium-voltage cable housings, as some models have suggested their working lifetime to be on the order of 300 years under standard operating conditions[4,5].

Beyond manufacturing of polymerized polymer, polyethylene can be modified post-manufacturing with processes like chemical crosslinking, which increases the overall strength of the backbone. Crosslinking is the process which neighboring backbones are chemically bonded together via carbon-carbon linkages. Large advancements in the production of crosslinked polyethylene can be attributed to its versatile use in cable insulation and jackets. With no effect on the dielectric properties of polyethylene, crosslinking reduces polymer flow while increasing the softening point to allow for higher operating temperatures[6]. The versatility of polyethylene, crosslinked or not, means this polymer is used widely and, in some applications, expected to maintain its performance for decades. Yet, it is clear that polymer products weather under environmental conditions, which reduces the products working lifetime[5].

Chemical forms and mechanical properties have been used to monitor how various aging conditions such as temperature, radiation, and solvents affect the lifetime of polyethylene. Independently, these have shown trends such as chemical transformations (i.e., crosslinking, chain scission and oxidation of the backbone, changes in molecular weight distribution), phase separation and lamellar thickening resulting from aging. Chain scission is the process where carbon-carbon bonds are broken into neighboring radicals. Any process that causes a neutral atom to lose electrons is known as oxidation and serves

as the method for changing the chemistry of polymers over time. Oxidation, which typically results in the incorporation of oxygen in to the polymer backbone, is a step that leads to chain scission via radical oxygen forming a new bond with carbon and breaking a bond holding the chain together. Although much progress has been made towards understanding these phenomena, there have been limited attempts to develop an overall polymer lifecycle where rates of aging indicators such as chemical crosslinking, chain scission and oxidation are integrated into a single timeline.

While there is limited understanding of extruded polyethylene, previous studies have worked to predict the failure of coating materials[7]. These epoxy-based coatings act as a protective layer on a metal surface, much like extruded polyethylene cable insulations. Typically, computer models examining breakdown as solely physical phenomena of penetrant diffusion through a multi-property barrier over some period. Although this approach examines rates of penetration, it treats the coating as a static, unchanging material, when in reality mechanical stresses are continuous, such as the strain induced by heating and cooling. Extruded polymers exhibit similar mechanical properties to these coatings, as they have low permeability, high flexibility and chemical resistivity. The large difference arises at a molecular level, where polymers are considered to be long chain hydrocarbons held together with intermolecular forces, whereas epoxies are cured to include chemical crosslinks. Dispersive forces are the governing intermolecular force between hydrocarbon chains, where instantaneous dipoles proportional to chain length cause folding and assembling of these extended chains[8]. By understanding these

differences, the predictive models used for the failure of coatings may be modified and applied to those of extruded polyethylene and similar plastics.

To date, many studies of coating degradation had been focused on the material's ability to maintain its engineered application with a lot of focus on the mechanical stability[9,10,11,12]. Yet, integrating chemical approaches to understanding polymer breakdown has not been fully incorporated even though the nature of the mechanical changes seen in aged polymer samples can be explained by chemical changes. For example, increasing brittleness of polymers arise from chemical crosslinking and loss of low molecular weight species which decreases mobility of hydrocarbon chains[9,12,10]. Similarly, chain scission reactions decrease polymer average molecular weight and thus decrease overall strength[12]. Therefore, developing a strategy that bridges the analytic approaches of engineers and chemists would further solidify the theories governing our understanding of polymer breakdown.

The aging of plastics is generally evaluated in terms of the overall product rather than a set of individual processes that may be occurring sequentially or in parallel. After connecting the ways in which chemical and physical monitoring complement each other, it is important to develop a timeline that predicts what processes are happening with given aging parameters. Here, we will survey the literature with the goal of presenting a timeline of polymer breakdown. Specifically, this predictive timeline will focus on environmental thermal degradation. While other environmental factors may be relevant for other applications (e.g., photon irradiation), thermal stresses are experienced in a wide

range of polyethylene variable and the timeline we set for thermal degradation can inform other degradation processes. In the specific case of a nuclear power cable, we assume the working location to be protected from sunlight and rain, but at elevated temperature from surrounding sources. By understanding a timeline of breakdown, we can begin to design strategies for evaluating polyethylene, among other materials, as we work toward a predictive model of failure of the cabling.

1.2 Understanding the Polyethylene Design

It is critical to understand polymer make-up and the details of the native structure in a pristine, unaged sample. Moving beyond bulk properties such as hardness or opacity, polyethylene at the microscopic level is made of millions of dynamic hydrocarbon chains. Evaluating polyethylene with this microscopic lens, rather than as a homogeneous, unified material, is important to better understanding how plastic characteristics change over time under various environmental stressors.

Polyethylene, the simplest of all polymers, has been primarily chosen as the base material used in electrical insulation. Many existing forms of polyethylene are classified by their density and melting point, which are dependent upon the degree of crosslinking, average molecular weight distribution and crystallinity within the polymer. The most common forms include very low density (VLDPE), low-density (LDPE), linear low-density (LLDPE), crosslinked (XLPE), high density (HDPE), and ultra-high density (UHDPE). Formation of the initial crystalline structure of the polymer is heavily influenced by the extrusion process of the film, where both processing temperature and cooling gradients

kinetically govern crystallization. These folded, high-density crystalline areas (known as lamellae) are surrounded laterally by areas of unorganized, weakly packed amorphous polymer. The lamellae are then separated by an anisotropic disordered phase, which is of the lowest density as suggested by investigation with Raman spectroscopy[13]. Wide-angle x-ray spectroscopy (WAXS) has been used to estimate a mean distance of 300-350 Å between neighboring lamellae in laboratory crystallized samples[14]. Studies have shown that a critical hydrocarbon chain length of at least 150 CH_2 units is needed for chain folding lamellae formation of 90-100 Å in thickness[15]. With a relatively low torsional barrier of 2-3 kcal mol^{-1}, chains have the ability to rotate between *gauche* and *trans* conformations[16, 17]. It was also suggested by simulations that chains of >60 CH_2 units favor the *trans* state when comparing torsional, bond angle deformation (repulsive) and van der Waals energies (attractive)[15].

With time, new processes for polyethylene film production have created materials with higher crystallinity, a lower degree of chain branching and increased processing efficiency. Typically, a low pressure, Zeigler-Natta process of polyethylene production yields high levels of crystallinity, whereas high pressure, free radical catalyzed processing yields higher chain branching and lower crystallinity[18]. Crosslinked polyethylene is the product of secondary processing of polyethylene, where the sample is either subjected to peroxides or an electron beam that induces chemical crosslinks in the backbone. To form polyethylene sheets, an extrusion process is used where plastic pellets are melted and forced out of a die, which is quickly cooled to maintain a sheet structure. A modified version of this process, called “overjacketing”, directly applies the formed

film onto a metal cable which can be layered with other materials[19]. During the extrusion process, an observed directionality to the polymer surface can be observed on the micro scale, which has been shown to intensify after exposure to elevated temperatures[20].

1.3 Characteristics of a Good Barrier

At a fundamental level, the goal of insulative barriers are to both stop dielectric breakdown via electron or ionic charge transfer, as well as separate environmental contaminants, such as salts, from reaching the conductive core. The dielectric constant is electric permeability of a material to that of free space (vacuum)[21]. These barriers also serve an indirect chemical purpose of reducing the amount of oxygen available to react with carbon radicals deeper within the polymer. Although the surface is free to react with oxygen, limiting oxygen permeation greatly extends the lifetime of a cable under the principle of maintaining its original chemical structure. Understanding the natural processes that control a plastic's ability to act as a barrier is the foundation for being able to model a timeline of insulative breakdown. It is instructive to understand the process behind permeability of gases and liquids to polyethylene barriers. Within the work herein, we make a general assumption that if a species can penetrate and cause dielectric breakdown of a polyethylene insulator (i.e. allow electrical shorting), it is considered as a failed barrier.

1.3.1 Permeability

A penetrants ability to pass through a barrier is defined mathematically by its permeability. The process of these penetrants moving across a barrier is known as diffusion. Like many other materials, Fick's law (equation 1) of diffusion may be used to evaluate polyethylene:

$$J = -D\frac{\delta C}{\delta x} \qquad \text{(Equation 1.)}$$

where J is the flux in mol · cm^{-2} · s^{-1}, D is the diffusion coefficient, c is the concentration (mol · cm^{-3}), x is the distance traveled from the surface and $\frac{\delta c}{\delta x}$ is the concentration gradient along the axis. Since there is only a small pressure gradient between the polymer and cable substrate we are limited to looking at penetration as steady-state and diffusion-limited by the penetrant. Permeability values, however, shed great insight on the barrier properties of the polymer since they are dependent on physical characteristics of the plastic, such as its diffusivity. For a semi-crystalline polymer, the diffusion coefficient can be determined using equation 2:

$$D = \frac{D_\theta\, \alpha\, \eta}{\beta_1\, \tau} \qquad \text{(Equation 2.)}$$

Where D_θ is the diffusivity of the amorphous content, α is the amorphous material fraction, η is a penetrant-dependent factor, β is an 'immobilization' factor of the penetrant and τ is a 'geometric impedance' factor of the material. It is generally assumed that sorption of both gases and liquids does not occur in the crystalline phase, and therefore geometric impedance will be a function of the crystalline fraction present[22,23,24]. Based on equation 1 and 2, it becomes clear that when performing tests to evaluate barrier

properties, understanding how amorphous and crystalline phases change will ultimately determine the service life of the plastic barrier.

Polyethylene as a cable housing is exposed to two major classes of penetrants: liquids and gases under natural aging conditions. Typically, these are limited to water containing trace amounts of salts, oxygen and nitrogen. The permeability of liquids and gases to polyethylene has been extensively studied[12,23,15,26,27,28]. For example, permeability constants of polyethylene to *n*-propyl alcohol (0.49) is almost 1000-fold less than that to benzene (440), as expected due to polarity[22]. Tables 1.1 & 1.3 demonstrate that despite polyethylene's use as an insulative housing because of high chemical resistivity, even polar chemicals can permeate a pristine sample, given relatively moderate thermal conditions. P_o represents the permeability of a chemical to polyethylene, where a larger value indicates a higher degree of permeability. A larger P_o value also indicates less energy is required for the process to take place; E_p represents the amount of energy required for the penetrant to penetrate the polyethylene. As polyethylene structure begins to deteriorate during aging, these rates of permeation may increase further.

Table 1.1: Temperature-dependent permeability of various solvents to polyethylene. An increase in permeability is inversely proportional to penetrant polarity

Penetrant	Temperature (°C)	P_o	E_p (kcal/mole)
n-propyl alcohol*	21 38 54 74	.49 2.89 22.4 168	22.11

Ethyl Acetate*	21 38 54 74	16.6 83.3 378 1990	17.72
Benzene*	21 38 54 74	440 1585 4480 13700	13.27
Oxygen**	25	1958 E16	

* 1000 um sample thickness
** 50-75 µm sample thickness

Bent[22] demonstrated the polarity effect using new polyethylene bottles and solvents of varying polarity and found a logarithmic increase in penetration for both polar and nonpolar solvents (Table 1.1). Similar tests performed using attenuated total reflectance-Fourier transformed infrared (ATR-FTIR) spectroscopy suggest that the fast diffusion, D_1, (monomeric and dimeric water) and slow diffusion, D_2, (cluster and bulk water) may occur at rates of up to 1.69 E-8 $cm^2 s^{-1}$ and 3.19 E-9 $cm^2 s^{-1}$ in a polymer at 80℃[29]. Table 2 outlines these findings. This suggests that water may be able to penetrate through a 30 µm barrier (T_{Px}) in as little as 2 days at elevated temperatures[29].

Table 1.2: Temperature-dependent saturation times for polyethylene with water[29]

Temperature	D_1 ($cm^2 s^{-1}$)	D_2 ($cm^2 s^{-1}$)	T_{P1} 30 µm (Days)	T_{P2} 30 µm (Days)
20 ℃	4.78×10^{-9}	7.67×10^{-10}	7.26	45.3
40 ℃	5.92×10^{-9}	7.54×10^{-10}	5.87	46.1
60 ℃	4.24×10^{-9}	9.58×10^{-10}	8.19	36.2
80 ℃	1.69×10^{-8}	3.19×10^{-9}	2.01	10.9

1.4 Methods for Monitoring Aging

Although not explicitly stated in literature, most polymer monitoring encompasses chemical-level, or physical-level analysis[30–37]. Table 1.3 outlines the monitoring methods commonly used and their analysis at both chemical and physical levels. For example, carbonyl content (hydrophobicity, chemical reactivity, discoloration, conductivity) and molecular weight changes (outgassing monitoring, brittleness, mechanical tests, permeability) are indicative of chemical changes. and crystallinity (structural analysis, permeability, dielectric breakdown). The trends that arise from monitoring these categories gives the basis for our understanding and ability to predict how polymer insulators will perform in the future.

Table 1.3: Common monitoring methods for chemical and physical changes in polyethylene

Monitoring Method	
Chemical Changes	Physical Changes
Carbonyl Content[30–32]	
Hydrophobicity Chemical Reactivity	Discoloration Conductivity Brittleness
Molecular Weight Changes[32,38]	
Chain Scission Crosslinking Intermolecular Forces	Outgassing Elasticity Elongation to Break Permeability
Crystallinity[30,31,33–35]	
Chain Scission	Permeability Structural analysis Strength Dielectric breakdown

1.4.1 Carbonyl Content

Monitoring carbonyl content is one of the most common chemical indicators of polyethylene aging because of its effects on changing chemical reactivity, hydrophilicity, brittleness, permeability and melting point[39,40,37,41]. Chemical oxidation of the polymer backbone in the presence of oxygen leads to the breaking of carbon-carbon bonds, hydrogen abstraction and formation of carbon-oxygen bonds. These processes, however, begin to differ when oxygen availability is limited. At this oxygen-limited point, crosslinking becomes the dominant reaction[42,43]. Similarly, crosslinking has been attributed to increasing the brittleness of polyethylene samples and decrease of strain-at-break values[30,31,44]. Under sufficient oxygen environments, products of these peroxy radical reactions have been characterized by FTIR as ketones, aldehydes, esters and carboxylic acids[39,45–47].

The slow but consistent rate of oxidation of polyethylene at room temperature (20-30℃) serves as a model timeline for the testing of aged samples, although there are no literature studies at these temperatures due to the extremely slow rate. Oxygen induction is inferred to be a measurement of the time required for significant oxidation to occur at a given temperature[30,48]. Typically used with DSC, the exact chemical identity of the oxidation product is not known but is known to involve formation of carbon-oxygen bonds. Table 1.4 shows the simulated induction time of polyethylene under low temperatures, which estimates up to 113 years before the onset of oxidation at 25℃[49].

Table 1.4: Temperature-dependent oxidation induction periods for polyethylene[49]

Temperature (℃)	Induction oxidation time
25	113 years
50	759 days
75	38 days
100	45 hours

On the other hand, under anaerobic conditions, polyethylene has been shown to be chemically stable at temperatures up to 300℃[50]. Since the combination of oxygen and elevated temperature readily deteriorate polyethylene, a large volume of studies have been performed looking towards understanding the chemical reactions behind oxidation, however the generally accepted pathway for polyethylene is as follows:

Initiation

1- $RH + O_2 \rightarrow R\cdot + HO_2$

2- $R\cdot + O_2 \rightarrow RO_2\cdot$

3A- $RO_2\cdot + RH \rightarrow RO_2R + H\cdot$

3B- $RO_2\cdot + RH \rightarrow RO_2H + R\cdot$

Norrish Type 1 & 2 Mechanisms

4A- $RO_2H + R\cdot \rightarrow RO\cdot + OH\cdot$

Crosslinking

4B- $R\cdot + R\cdot \rightarrow R_2$

Scission

4C- $RHR + R\cdot \rightarrow R_2 + RH$

Thermally induced formation of radical sites react with oxygen to form an alkoxy radical[51,52]. Hydrogen abstraction then produces a hydroperoxide which undergoes a Norrish-style reaction to produce carbonyl and a hydroxyl radical. These Norrish reactions continue as the uniform hydrocarbon chains are slowly fractured into short segments which may be volatilized or exist as highly mobile chains within the polymer[34]. If two neighboring radicals are not consumed by oxygen, they may recombine and cause crosslinking amongst chains[22,37,41,31]. The rate of carbonyl formation becomes accelerated as radical content increases and regenerates. It can then be inferred that the formation of carbonyl groups in the polymer backbone proceeds physical changes that affect the long-term mechanical performance of the polymer, such as tensile strength, thus making carbonyl a good indicator for overall aging. These processes occur slowly at room temperature, but in as short as a few minutes at temperature exceeding the melting point of the polymer. It has also been discussed that an initial amount of surface hydroperoxide content exists in polyethylene, assisting in the formation of carbonyl[45]. Carbonyl, a general term, exists more specifically in oxidized polyethylene as aldehydes, ketones, carboxylic acids and esters.

FTIR is used to qualitatively assess carbonyl content due to its quick analysis and well-defined bands, as well as non-destructive nature. Table 1.5 outlines the characteristic absorbance bands which make up the carbonyl region of an FTIR spectra. Recent efforts have been made to increase to quantitative assessment of carbonyl content via an indexing method which offers more variability to the use of FTIR[54]. This indexing

normalizes the total area of the carbonyl region from 1680 - 1720 cm^{-1}, to a carbon-hydrogen wagging band from 1320 - 1400 cm^{-1}. Typically, the carbonyl bands are monitored as a whole due to their close proximity and spectral overlap, however efforts have been made to identify the individual contribution of specific functional groups[39].

Table 1.5: identification and assignment of functional groups located in the carbonyl region of an FTIR spectra

Functional Group	IR Band (cm^{-1})
Aldehyde C=O Stretch	1740 – 1690
Ketone C=O Stretch	1750 – 1680
Ester C=O Stretch	1750 – 1735
Carboxylic Acid C=O	1780 – 1710

1.4.2 Molecular Weight

The two main types of plastics are thermoplastics and thermosets, where one gains its strength through intermolecular forces, and the latter through chemical bonds. Although thermoset plastics offer more strength and chemical resistivity, thermoplastics are more flexible and can be recycled. There is a natural dispersion of molecular weight amongst the chains, with higher molecular weight segments having larger intermolecular forces. Chain length, therefore, is directionally proportional to melting point and thus is an important factor in understanding how polyethylene behaves under a range of temperatures. Figure 1.1 outlines the 5 major temperature dependent states of polymers: glassy, glassy transition (T_G), rubbery, melt and viscous.

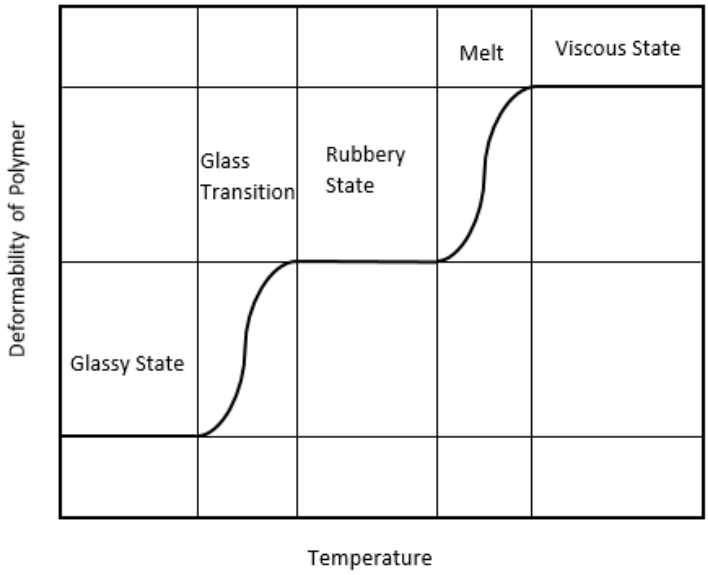

Figure 1.1: Physical states of polymers as a function of temperature.

Volatile organic compounds (VOC's), low-molecular weight carbon compounds, are produced when chain length is reduced. This process can occur either during plastic production, or chemically through chain scission. Under heating, enough energy allows these hydrocarbons to overcome the attractive forces and leave the lattice (outgassing) or disrupt the surrounding chains (Figure 1.2).

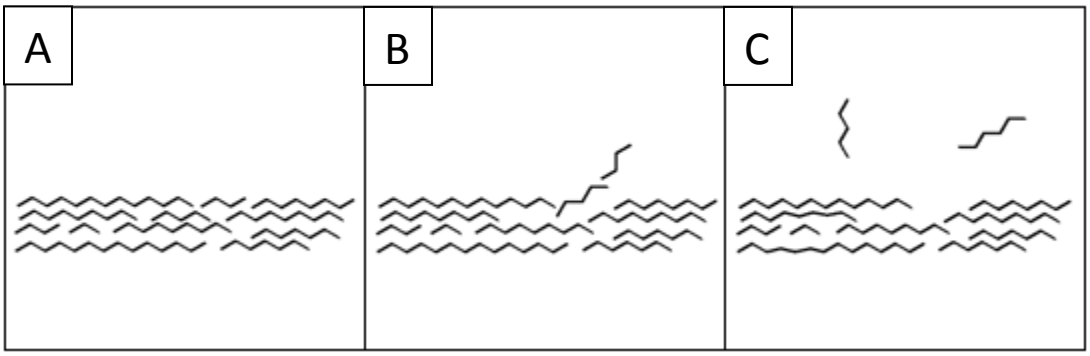

Figure 1.2: Panel A: the first few layers of hydrocarbon chains in the polymer. Panel B: outgassing of VOC's create voids in the polymer which allow penetrants into the surface.

Panel C: VOC's trapped in the polymer create separations because of increased thermal energy.

VOC's can then be subdivided based on volatility temperature seen in Figure 1.3, where under ambient conditions, both very volatile organic compounds (VVOC's) and some VOC's compose outgassing products[55]. To keep consistent with environmental degradation, we will focus on the products containing VVOC's and VOC's, since semi-volatile organic compounds (SVOC's) and particulate organic matter (POM) are formed at or above combustion temperatures of polyethylene.

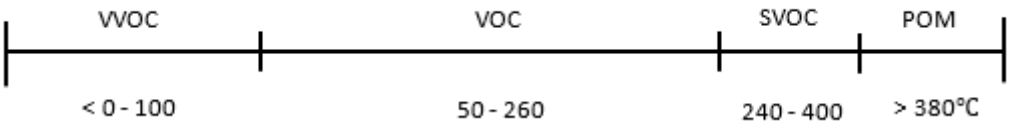

Figure 1.3: Identification of outgassing species at varying temperatures.

VOC composition includes: aldehydes, alkanes, alkenes, amines, aromatics, esters, ketones, and other organics[56–58]. Typically, these are assessed in terms of atmospheric pollution due to their widespread production in the burning of organic compounds[57,59], however, they also play a role in the breakdown of plastic barriers. Laurent et. al. demonstrated that diffusion of VOC's through the polymer causes formation of cavities where electric discharge occurs[60]. These physical voids in the polymer also allow for oxygen and water to penetrate further into the surface.

Thermogravimetric analysis (TGA) is used to understand the physical and chemical properties (e.g. VOC content) of a polymer upon heating under oxygen or nitrogen. As stated previously, when the chain length decreases to < 60 carbon units long, the change in conformation further weakens the intermolecular forces between chains, and therefore would be more susceptible to volatilization[15]. TGA of polyethylene has been shown to produce hydrocarbon chains between 1- 70 CH_2 units long, when heated to 600℃ at 0.5-20 ℃/min under nitrogen[61]. Most products recorded were 1-hexene and propene resulting from self-scission after radical formation. These low molecular weight chains can then become volatilized between room temperature and 65℃. The rate of volatilization occurs much faster upon initial exposure to elevated temperature than after an extended period of time. McCaffrey demonstrated that the rate of mass decrease of a sample exposed to 350℃ accelerated until reaching a maximum during the first 50 minutes of exposure, followed by a deceleration where high molecular weight species were lost[62]. This initial period accounted for a loss of about 20% of the total molecular weight[62].

1.4.3 Crystallinity

Amongst the several forms of polyethylene (e.g., XLPE or LDPE) crystallinity ranges from 30% - 80% depending on the form and extrusion process. For example, extruded LDPE film is approximately 50% crystalline and 50% amorphous[18]. Although chemically identical, both sections offer significantly different barrier properties. Murthy et.al. defined amorphous as a structure without long-range three-dimensional order[2]. It is generally assumed that sorption of both gases and liquids does not occur in the crystalline phase, and therefore, the amorphous regions have an important role for consideration in

the behavior of the barrier[22–24]. Figure 1.4 A represents a cross section of the crystalline area, where ordered lamellar stacks are composed of hydrocarbon chains with periodic folds at the top and bottom of the stack[63]. The amorphous region, seen in Figure 1.4 B, is composed of disordered hydrocarbon chains which exist between ordered lamellae.

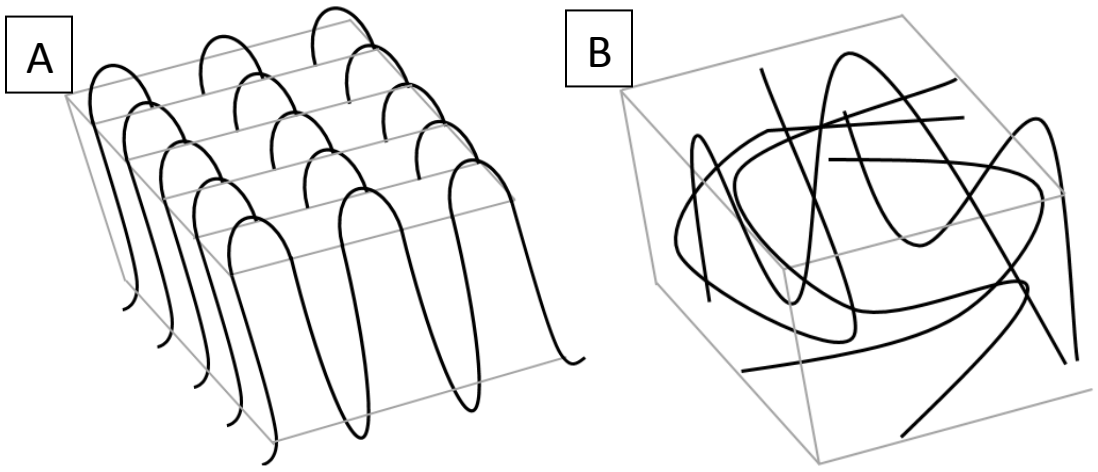

Figure 1.4: Panel A: diagram of a cross section of polyethylene in a crystalline lattice. Panel B: diagram of a cross section of polyethylene in the amorphous region.

The nature of the amorphous region is difficult to elucidate due to its lack of order. Common x-ray crystallography studies not suitable for determining structure of the amorphous sections because of the lack of order. In addition, electron microscopy, although able to distinguish individual atoms, is not suitable due to the low molecular weight of polyethylene that can move under the energy of the beam. Despite the apparent lack of order, the amorphous region can be subdivided further into a ‘stack’ region and interlamellar region (between layered hydrocarbons), which both contribute to the sorption of water and gases[63,64]. The low-density interlamellar region of disoriented

chains connect neighboring lamellae and can be expanded as the result of hydrating or heating[64]. The increase in the lamellar spacing is probably due to an expansion of the interlamellar amorphous domains caused by the temperature and diffusion of water.

The crystalline phase can be considered a combination of orthorhombic and monoclinic unit cells (Figure 1.5), with the orthorhombic being more stable[63] and chains being oriented in the *trans* configuration[15]. Due to the dynamic nature of hydrocarbon chains, it can be assumed that heating and mechanical stress cause consistent changes in the overall crystallinity of the polymer, which was thoroughly investigated by E. W. Fischer[17,65]. Upon heating, polyethylene demonstrates a linear decrease in crystallinity of 10% until temperatures approach the melting point, where a steep loss is observed until melting[14,36,66]. Small angle x-ray scattering (SAXS) tests reveal an increase in surface disorder at the melting point due to the creation of surface vacancies and increasing roughness[65]. This is a common technique for bulk characterization of polymers, which indicates both the long spacing of lamellae (space between neighboring lamellae) and degree of crystallinity[67]. Measurements were performed by heating a sample from below T_g to above melting and back while monitoring the scattering of x-rays through the sample. This produced two phase curves, one during heating, and the other during cooling. Similar studies of cyclic heating of polyethylene beyond its melting point increased crystallinity when returning to room temperature[14]. This is an example of an α-relaxation process within the polymer, where the polymer transforms the structure from an unstable state to a more stable one[65,68]. If a second heating cycle is introduced, the new

phase curve then follows the previous cooling curve in reverse, with either an increase or decrease in crystallinity to follow, which was not fully understood[67].

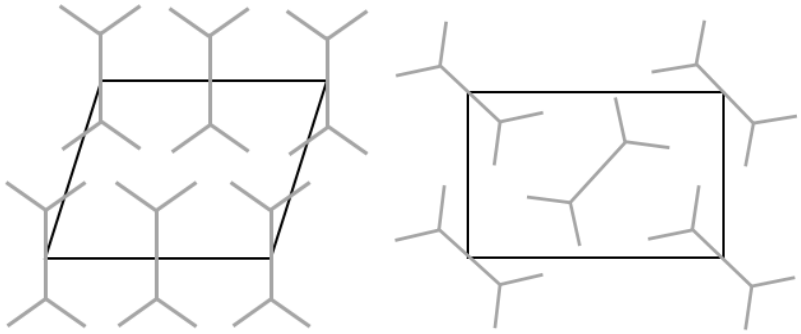

Figure 1.5: The orthorhombic (left) and monoclinic (right) structure of polyethylene. Images are looking at the hydrocarbon chain end-on.

Other physical changes to the polymer structure occur that influence crystallinity. Lamellar thickening is a process which the stack height increases perpendicular to the lamellae, while decreasing in lateral width. It has been observed to occur irreversibly at temperatures above 100℃[14]. This both increases of the number of lamellae stacked in the crystalline cell, but also increases interlamellar spacing where solvents and gases may be able to penetrate. Other theories suggest that at temperatures of 100℃, creation of localized 'kink' defects (gauche transitions) in the crystal create decreases in lamellar density, allowing deeper penetration of electrons in scattering studies[65]. With these voids having an average length of 8 Å, we can assume oxygen (van der Waals radius: 1.52 Å) and water (van der Waals radius: 2.8 Å) can penetrate between the crystal lamellae.

A relationship between crystallinity and molecular weight also exists. For example, it was reported that an increase in polymer crystallinity was observed with decreasing molecular weight[36]. This is the result of smaller, non-volatile species packing more easily into a lattice structure, but also increasing permeability with decreasing molecular weight. The relationship between molecular weight and polymer packing underscores the importance of monitoring crystallinity in tandem with molecular weight characterization to give a better indication of aging and permeability.

1.5 Developing a model of polymer aging

It is apparent that understanding the failure of a cable housing includes chemical processes such as oxidation, chain scission which results in the reduction of average molecular weight. Although this is a chemical process, the effects are typically reported as explanations for physical changes (e.g. elongation to break, ductility and ultimate tensile strength)[9,30–32,37,69]. Together, these control the permeability of an insulative sheath and therefore the robustness of the barrier application.

There have been no attempts to model a complete breakdown mechanism for cable housings with an understanding beyond 3-5 years of aging. A recent model for the breakdown of coatings on metals was developed by Hinderliter *et .al*., where a homogeneous polymer coating has pores that extend some distance into the surface, along with vacant and saturated pockets[7]. These pockets, or voids, have also been seen in the study of polymers[64]. The coating also has an area of pristine polymer, where it is

assumed no penetrants have been transported from the exterior. The current model suggests that oxidation of the surface and inner pores increases hydrophilicity of the polymer interface. In a wet environment, this can then draw water into the pore and application of thermal stress advances the depth of the pore, as it has been seen to increase interlamellar spacing[64]. In a dry environment, crosslinking of the polymer surfaces create brittleness, which in combination with naturally occurring lamellar thickening and mechanical stress advances pore size. The advancement of the pores can lead to the failure of the cabling. Electrical arcing can then occur in proximity of other conductive materials or a high humidity environment. Similarly, the increase of point defects within or at the surface of the cable can cause electrical treeing, where an electrical gradient force either water or burns through the housing, creating a tree-like pattern[4]. With working conditions of some cable exceeding temperatures of 80℃, exposed to water and sunlight, the accelerated aging of these cables decreases working lifetimes to less than 30 years[5].

In our model, however, we assume cables are under standard working conditions. This includes being inside a structure protected from ultraviolet radiation and rain water, but exposed to temperatures of 60 - 100℃, with varying humidity and ambient oxygen content.

Interestingly, oxidation at temperatures where diffusion becomes rate-limiting may experience retention of barrier properties for longer than those oxidized at lower temperatures as seen in Figure 1.6. Since the diffusion of oxygen and water into pristine

polymer is known to occur as a rate[29] and oxidation only occurs in the presence of oxygen, an oxidative gradient may exist as it has been seen in polyethylene sheets[39] and rubber products[70]. In a cable with no experience of mechanical stress, permeability to oxygen, a key reagent in the oxidation process, has been reported to decrease with increased oxidation and becomes impermeable to oxygen[70]. This creates an impermeable barrier near the surface, leading to a near-anaerobic and unoxidized environment at the insulator core.

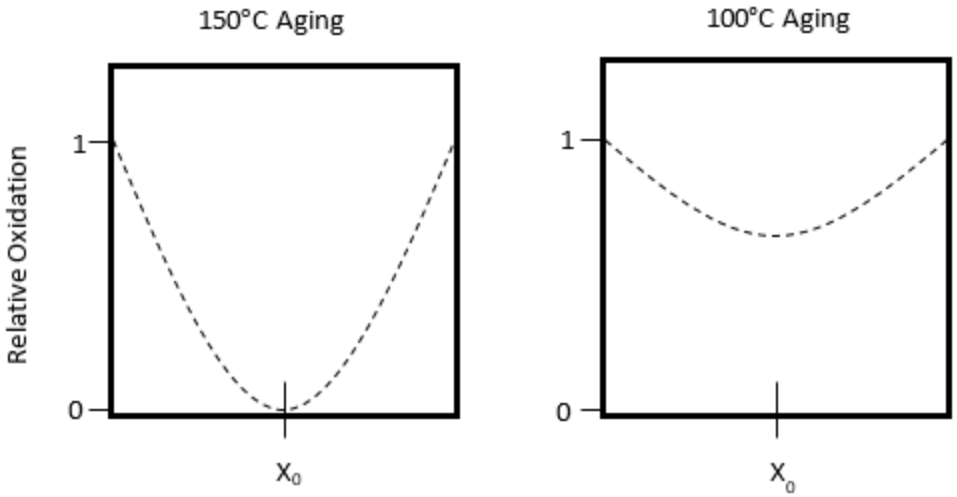

Figure 1.6: The relative oxidation of a rubber at 150℃ (left) and 100℃ (Right) temperature. Rapid oxidation of the surface decreases permeability to oxygen at higher temperature. Similar results are seen in polyethylene sheets[39].

The hypothesized oxidation gradient must be considered when making conclusions about the quality of an insulative barrier assessed under accelerated aging conditions, as a lack of homogeneity would decrease the reliability of measurements taken of a surface (FTIR) versus the bulk material (Differential scanning calorimetry).

The literature collected to produce the timeline in Figure 1.7 was only included in this timeline if it fell within several specific guidelines. The aging conditions of the polyethylene must have only included thermal treatment between room temperature and 120°C. Temperatures above 120°C cause LDPE to melt, and thus change the barrier properties of the sample, therefore, data on TGA analysis was not included since it is typically collected at temperatures exceeding 200°C[30,71]. In previous work, we have shown that photooxidation of polyethylene using UV radiation occurs within hours of exposure[38,54,72], in contrast to weeks for the thermal oxidation of polyethylene, therefore masking thermal effects we are looking to model. Furthermore, since we assume a simulated cable housing, an outer plastic layer protects the inner polyethylene from photooxidation.

Currently, surveying the kinetic and thermodynamic rates of thermal oxidation has not yet been performed. Although the precision of the estimates cannot be quantified, we believe the chronological process of aging and proposed rates to be accurate in accordance with the literature.

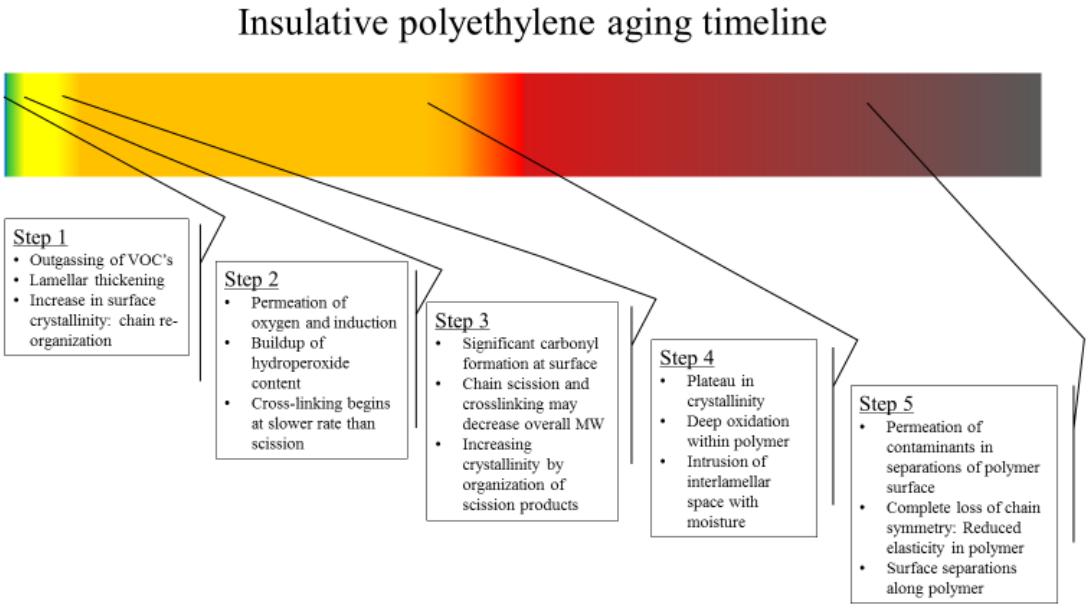

Figure 1.7: Predictive timeline for the aging of insulative polyethylene barriers. The figure has been scaled relative to the expected rate of aging.

Pristine Polymer

Our understanding from the degradation of coatings along with that of permeability through polymers can be applied to the analysis of polyethylene cable housings to give us a timeline of chemical and physical changes induced by thermal aging. As discussed previously, polyethylene sheets are made of layers of packed polymers in either a crystalline or amorphous phase. Between these layers exists interlamellar spacing where water or other gaseous species may exist, with hydrocarbon chains extending between lamellae[25]. More importantly, due to the dynamic nature of mobile polymers, diffusion channels within the polymer are temporary, meaning lamellar movement may leave some sites accessible only at certain times[25]. Naturally occurring voids in the polymer are randomly scattered throughout the polymer, extending through multiple lamellar stacks.

We propose the following timeline for polyethylene cable degradation represented in Figure 1.7.

Step 1

The increased temperature allows initial conformational stress of the polymer to relax and rearrange into the crystal lattice, increasing crystallinity of the polymer. The increased thermal energy allows VOC's to escape through both the amorphous phase and temporary micro separations formed during polymer expansion at a loss rate of 0.05% wt/day. Lamellar thickening draws surrounding hydrocarbon chains, both increasing the size of lamellae and interlamellar space (at the same rate). This is represented by the blue portion of the scale in Figure1.7.

Step 2

Permeation of oxygen into the surface via amorphous areas begins as outgassing decreases void content increases. Native hydroperoxide content continues to increase in concentration and random chain scission increases radical content and decreases molecular weight[45]. Cross linking begins to occur via radical recombination; though the overall molecular weight of the polymer remains lower than before the aging process. An explanation could be the inability for neighboring radicals to recombine due to distance or competing reactions with oxygen. This is represented by the green portion of the scale in Figure 1.7.

Step 3

Increasing crystallinity of the polymer as lower molecular weight species produced via scission re-pack into the lattice. Radicals formed from chain scission compete between two processes: carbonyl formation and Norrish reactions with crosslinking from radical recombination. Both processes begin to increase molecular weight and brittleness of the polymer by decreasing symmetry of long chains. This is represented by the yellow portion of the scale in Figure 1.7.

Step 4

The rate of increasing crystallinity caused by packing of low molecular weight chains begins to plateau. Oxidation increases deeper in the polymer surface and changing hydrophilicity draws water into the surface through amorphous regions, or voids created during the outgassing of VOCs. Intrusion of the interlamellar space with moisture further separates lamellae. We hypothesize the rate of cross linking and chain scission begin to equilibrate. This is represented by the orange portion of the scale in Figure 1.7.

Step 5

Reduction of the mobility of hydrocarbon chains through cross links and branching stabilizes voids which penetrate the polymer surface. Work done on understanding the formation of crack growth in polyethylene cables has shown that upon thermal stress, crack growth propagates quicker in low-molecular weight samples, but slows in the presence of crosslinking[10]. Although less susceptible to thermally-induced fracture, the significant decrease in elastic modulus makes the polymer more susceptible to fracture from mechanical forces. The fracture proceeds through the weakest elements of the

structure, *i.e.*, through the boundary between adjacent microfibrils and the amorphous layers between subsequent blocks of the microfibrils[73]. This leads to complete failure of the cable as intrusion of contaminants close to the core leads to electrical treeing and shorting of the cable. This is represented by the red portion of the scale in Figure 1.7.

The polymer aging timeline above has several important gaps in knowledge about the role of crystallinity as a factor which influences the barrier properties of the insulative PE layer. The surface of the insulative layer is the primary subject of oxidation and thus controls the rate of oxidation through the rest of the layer. The combination of effects such as temperature, oxygen content, humidity and chemicals all compete changing the reactivity and physical characteristics of the PE. Although DSC works well for determining the bulk crystallinity of polymer samples, it is destructive, requires a large amount of sample and does not give insight about surface crystallinity. Therefore, it is the goal of this thesis to develop an ATR-FTIR method to determine the crystallinity of low-density polyethylene after thermal oxidation simulating the working condition of some medium-voltage power cables.

Furthermore, a novel method for understanding the physical breakdown of medium-voltage power cables was developed. It is hypothesized that growing phase separations in the PE surface, including the formation of pores into the insulation, ultimately lead to breakdown of the insulating properties of the polymer and shorting or failure of the cable. Current methods for evaluating/visualizing degradation include aggressive treatment with NaOH and labeling with methylene blue dye, but this process is time

intensive and requires extensive treatment of the polymer. Therefore, it is the goal of this study to design a more efficient method for labeling the structural changes of the polymer (e.g., capillary pores) using gold nanoparticles (AuNPs). With the use of electrical impedance spectroscopy (EIS), we hypothesize that charged gold nanoparticles can be driven into film pores and then imaged with transmission electron microscopy to elucidate pore structure.

Chapter 2. Validation of Predictive Aging Model: Relating Physical and Chemical Changes to Barrier Properties

ABSTRACT

To validate the proposed timeline, an aging study of polyethylene films (30 μm) was performed. Films were aged at 110°C for 24-hour periods in an oven and carbonyl content, a common aging indicator, was monitored. Accelerated growth of the carbonyl, monitored with ATR-FTIR was quantified using an indexing method. An ATR-FTIR crystallinity monitoring technique was also developed and revealed a 3-phase change of crystalline structure upon thermal aging we attribute to lattice reorganization, chain scission and chemical crosslinking. To better visualize the hypothesized pore formation in the polyethylene, which follows aging, EIS was used to saturate pores with gold nanoparticles before elemental analysis and imaging with SEM. EIS analysis suggests a breakdown in the barrier properties of polyethylene, and the existence of these pores large enough for the flow of chloride ions through the film, but not ≈5 nm gold nanoparticles.

2.1 Methods

Cleaning: All glassware used was treated with aqua regia and rinsed with MilliQ water (18.1 MΩ, EMD Millipore).

Accelerated aging of PE: LDPE films made by blown extrusion were obtained from Goodfellow USA and were 30 µm thick, biaxially oriented and transparent. To age, PE films were suspended in an oven at 110°C and periodically sampled in 24 h intervals (24, 48, 72, 96, 144, 192, 264 & 336 h). Samples were analyzed with ATR-FTIR to observe chemical changes within the films. Samples were aged until FTIR indicated significant oxidation, or film condition deteriorated upon handling.

ATR-FTIR Analysis: Infrared spectra were obtained in the absorbance mode using a Nicolet iS10 FTIR spectrometer (Thermo Scientific) equipped with a diamond attenuated total reflectance (ATR) accessory. All spectra were collected in OMNIC using a range of 600 to 4000 cm^{-1}, resolution of 4 cm^{-1}, and 64 scans. Triplicate scans were taken for each film and background was collected before every scan after cleaning the crystal with methanol.

IR Spectra Data Analysis: Oxidation was quantified through analysis of the ATR-FTIR spectra. Specifically, the carbonyl band (around 1720 cm^{-1}) was baseline subtracted and the fit band was integrated. A normalization band was also fit and integrated to find the area under the band. This normalization accounts for variability in the amount of polymer on the ATR crystal. For polyethylene, the normalization band was from CH_2 wagging

and CH_3 bending (~1320-1400 cm^{-1}). Subsequently, the oxidation is reported as a carbonyl index, which can be calculated based on equation 3:

$$Carbonyl\ Index = \frac{A_{Carbonyl}}{A_{Normalization}} \qquad \text{(Equation 3.)}$$

where $A_{Carbonyl}$ is the area of the carbonyl band (~1720 cm^{-1}) and $A_{Normalization}$ is the area of the normalization band.

Crystallinity was similarly quantified through analysis of ATR-FTIR spectra. A distinguished IR bending doublet band in the 1472 - 1456 cm^{-1} has been characterized in previous literature[74–76] and methods have been evaluated for determining polyethylene crystallinity[76,77]. The orthorhombic (crystalline) band located between 1472 cm^{-1} was compared to the sum of the integrated intensities of the gauche and trans (amorphous) bands[76] between 1456 - 1466 cm^{-1} . After deconvoluting peaks using Omnic software, percent crystallinity can then be calculated using the equation 4:

$$X = 1 - \left[\frac{\left(1-\frac{I_{cr}}{I_{am}}\right)}{\left(\frac{1.233}{1+\frac{I_{cr}}{I_{am}}}\right)}\right] \times 100 \qquad \text{(Equation 4.)}$$

where X is the percent crystallinity component, I_{cr} is the integrated intensity of the crystalline region, I_{am} is the sum of the integrated intensity of the amorphous region and 1.233 is the calculated intensity ratio of I_{cr}/I_{am} that has been empirically determined within the literature[75].

A 4-peak Gaussian deconvolution method was developed using Omnic software, where the peaks located at ~1471, 1461, 1457 and 1443 cm^{-1} were used to populate the region between 1520-1385 cm^{-1}. There have been 4 main peaks within this crystallinity doublet which have been noted in the literature: orthorhombic wagging deformation (crystalline, 1471 cm^{-1}), gauche wagging deformation (amorphous, 1461 cm^{-1}), hexagonal packed deformation (amorphous, 1457 cm^{-1}) and a broad shoulder peak[78,79,80].The commonly observed broad shoulder peak at 1443 cm^{-1} was not used in calculations, and all other peaks were removed as they were determined to be noise-induced. Another processing software, IGOR pro, was also used for the crystallinity calculations, however, this analysis resulted in large inconsistencies in the fitting of spectra that were also analyzed with Omnic, therefore, Omnic peak fitting was the preferred analysis tool. For further information, see Appendix.

Differential Scanning Calorimetry

Measurements were performed using a DSC Q 1000 (TA Instruments) on Tzero pans. All sample weights were between 1 - 2.5 mg. A normalization heating cycle from 20℃ - 150℃ at a rate of 10℃/minute was performed, followed by a cooling cycle, then a second heating cycle.

Processing was performed using TA Instruments Universal Analysis 2000. The second cooling cycle was used for crystallinity measurements. A sigmoidal horizontal baseline was used, and peak area was integrated from ~30℃ - 105℃, which represented the onset of changing heat flow until the end of the freezing peak. The integration of the

downwards heating peak, with reference to the H_f of 100% crystalline polyethylene, 293 J/g (TA Instruments).

Gold nanoparticle synthesis: A modified Turkevich method was used for preparing sub -10 nm AuNPs[81,82]. A 100 µL reduction solution containing 50 µL of sodium citrate (50 mM, Fisher Scientific) and 50 µL tannic acid (25 mM, Alfa Aesar) was prepared from stock solutions and injected into 10 mL of Milli-Q purified water (18 MOhm cm specific resistance, EMD Millipore, Burlington, MA) in a 25 ml glass screw-top vial. After heating to a boil, 1 mL of chloroauric acid tetrahydrate (1.1 mM, HAuCl4, Aldrich) was injected. It was found that lower temperatures favored larger particles to form. The solution immediately turned orange-brown and was stirred while heat was reduced to below boiling. After 2 minutes, the solution was removed from heat and let cool overnight to room temperature. The solution darkened slightly to a deeper color after 12 hours. The solutions were then ultracentrifuged at 350000×g for 20 minutes, rinsed with Milli-Q water and repeated once. Concentrate was collected, UV-Visible spectroscopy (Cary 5000) and TEM (Technai T-12) were then used to confirm the 4.9 nm size and stock solution concentration.

Nanoparticle characterization: A bronze colored solution was analyzed with UV-Vis spectroscopy and the nanoparticle solution had a maximum absorbance at 522 nm. Beer's law was used to calculate the molar nanoparticle concentration of with a molar absorption coefficient of 1.01E8 $M^{-1}cm^{-1}$ [83]. For example, a solution of 10x diluted nanoparticle solution with an absorbance of 0.453 yielded a solution concentration of 1.23E-8 M. UV-

Vis was performed on the solution 1 week later with no change in maximum absorbance wavelength, indicating stability for at least 1 week. Using UV visible spectroscopy determined concentrations, the solution was then diluted to 2.55 ppm immediately prior to EIS measurements.

The quantitative evaluation of the gold nanoparticle synthesis is seen in Table 2.1 TEM (Technai-T12) was used to image the nanoparticles to determine their diameter. ImageJ analysis of TEM images revealed an average size of 4.9 ± 0.9 nm. (78 particles)

Table 2.1: Quantitative evaluation of nanoparticle synthesis

Absorbance	EIS Solution Concentration (PPM)	UV-Vis Diameter estimation[83] (nm)	Synthesis Replicates	TEM Diameter	Standard deviation
4.12	2.55	5-10	6	4.9	0.9

Electrical impedance spectroscopy

The aged PE was placed between two H-shaped glass cells with Milli-Q water on one side and either Milli-Q water, 2.55 ppm AuNPs, or an AuNP precursor salt (1.1 mM, HAuCl4). Graphite electrodes (6", Gamry Instruments, Warminster PA) were used with a platinum wire reference electrode. The impedances were measured from 10 kHz to 0.01 Hz with a Gamry Reference 600+ potentiostat. A direct voltage of positive or negative 1.0 V was applied to the samples to drive nanoparticles or ions into aged thin film PE samples.

Although more information about barrier properties can be inferred from the circuit models, I am only treating EIS as a method for saturating the pores of aged plastics with

charged nanoparticles. Hence, the focus of analysis here will be only on the dielectric breakdown of the film after aging and understanding if nanoparticles may be present in the film. The citrate cap of the nanoparticles provides a negative charge that provides a driving force under the presence of a DC potential.

An equivalent circuit can be used to represent the EIS model in the form of a Randles Cell with a Warburg element, where R_S is the resistance of the electrolyte solution and R_{ct} is the resistance of charge transfer through the medium. C_{dl} is the double-layer capacitance, where charge builds up on the material and a Warburg element, W[84]. This equivalent circuit will be the basis for modelling EIS results, seen in Figure 2.0.

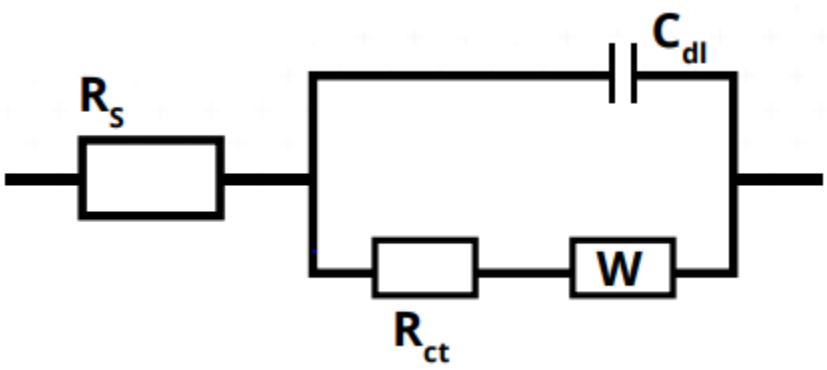

Figure 2.0: A Randles cell with a Warburg Impedance factor.

Due to the presence of the capacitors in an AC circuit, an imaginary component arises when considering the impedance (Z), where $Z_c = \frac{1}{J\omega C}$ and $Z_R = R$. The EIS therefore cycles through a range of frequencies which influence the magnitude of the resistance of the sample barrier.

All measurements presented were taken during a reference cycle with no applied voltage, after the indicated active cycle. This was done to ensure measurements show permanent changes to the sample.

Scanning Electron Microscopy

Imaging was performed using a JEOL JSM-6490LV SEM. Secondary electron imaging was performed under high vacuum. Backscattered electron imaging for elemental analysis was calibrated using copper tape at an acceleration voltage of 25 kV, spot size of 66 using aperture 2 of 3 and a working distance of 10 mm. Carbon coating was not performed on any samples as it would interfere with elemental analysis. INCA Feature software was used for all elemental analysis. All other imaging parameters are indicated under images.

Films were placed on carbon tape and wiped with a methanol wetted swab to remove surface debris or ions not trapped in the film.

2.2 Results & Discussion

2.2.1 Evaluating the Chemical Changes with ATR-FTIR

We used ATR-FTIR to evaluate the various chemical changes of PE thin films after aging samples at elevated temperatures (Figure 2.1). Two significant changes after thermal aging are present on the FTIR spectra. Growth of the carbonyl region between 1650 - 1760 cm^{-1} indicates oxidation of the polymer surface. The second change is seen between 1472 - 1456 cm^{-1}, where the ratio of crystalline to amorphous polymer is indicated.

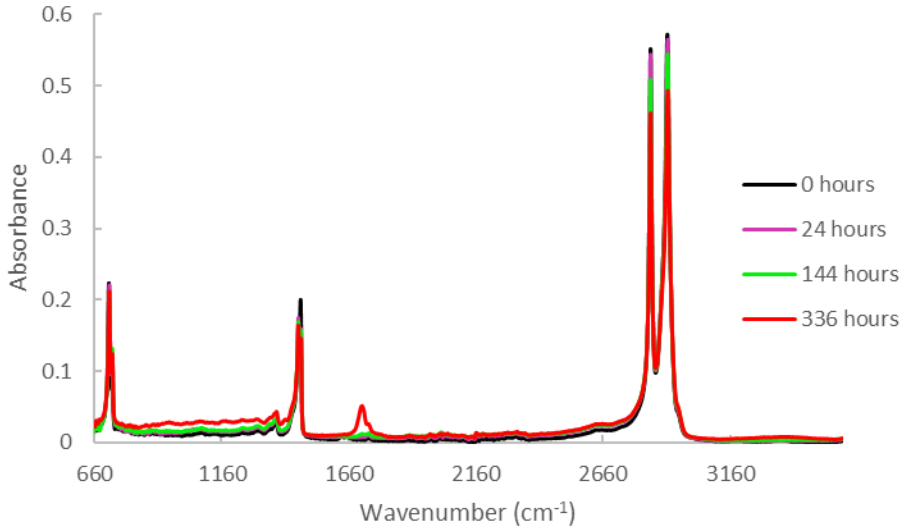

Figure 2.1: FTIR spectra of polyethylene after indicated aging period at 110℃.

Representative spectra are chosen.

2.2.2 Oxidation

The carbonyl region, an indicator for oxidation, indicates an initial growth of the band between 1730 - 1750 cm^{-1} (aldehyde[72]) during the first 144 hours of thermal aging, followed by rapid growth of the carbonyl band between 1690 - 1730 cm^{-1} (ketone/ carboxylic acid[72]) seen in Figure 2.2. The integrated area of these two bands were used to produce a carbonyl index with respect to the individual normalization bands from 1320 - 1400 cm^{-1}, seen in Figure 2.2.

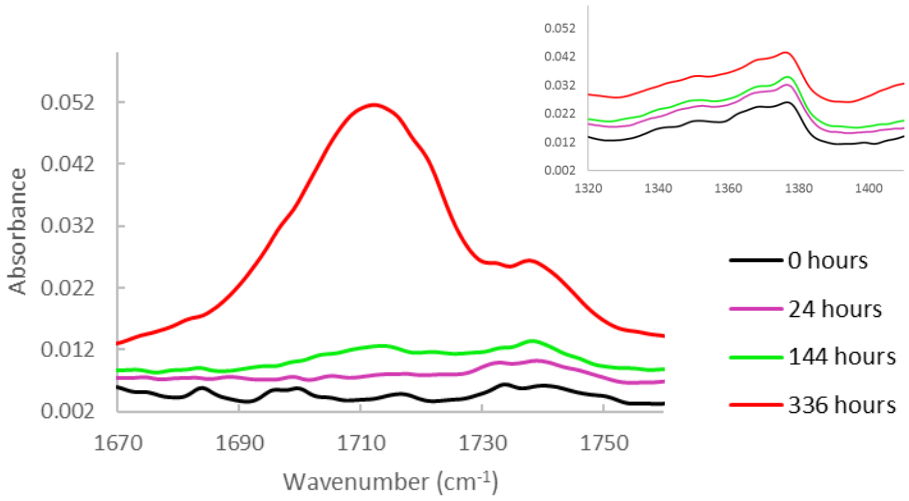

Figure 2.2: Expansion of FTIR spectra in both the carbonyl region (1690 – 1750 cm^{-1}) and normalization region (1320 – 1400 cm^{-1}) of polyethylene after indicated aging period at 110℃.

Computer simulations have also yielded similar results for the trend of auto-accelerated carbonyl formation of PE at 110℃[48], where an auto acceleration period is noted after a critical hydroperoxide surface concentration is achieved. Other studies contrast this hypothesis, however, believing the increasing availability of radicals from chain scission increases induction of oxygen which forms a carbonyl in the backbone[32]. This is then followed by steady-state decomposition as carbonyl production accelerates until it too reaches a steady-state. Figure 2.3 shows the carbonyl index where significant carbonyl formation is achieved by 192 hours of aging.

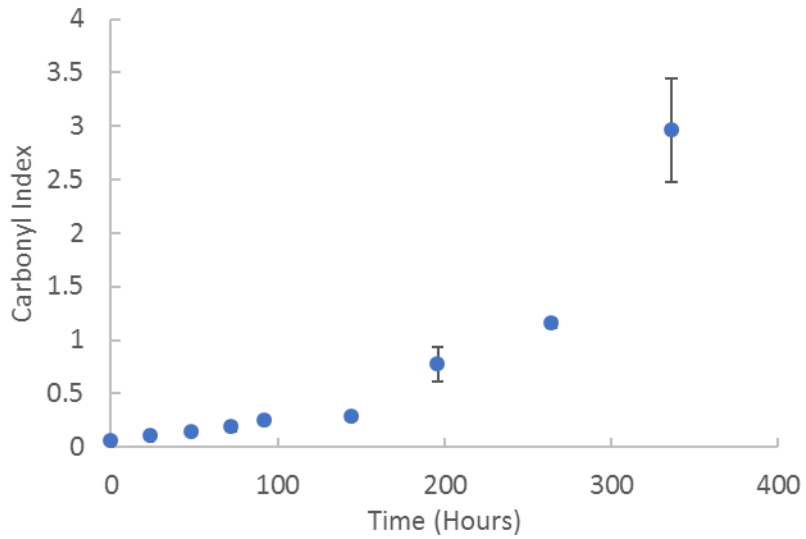

Figure 2.3: Carbonyl index for polyethylene after 14 days of aging at 110℃. Each point represents the average of 9 spectra, and error bars representing the standard deviation of each point.

2.2.3 Crystallinity

Two regions exist in an FTIR spectra of polyethylene that describe the ratio of crystalline to amorphous content. Although it is not a novel idea to study these regions, it has generally been done so at a qualitative level[16]. The 1472 – 1456 cm^{-1} doublet represents the amorphous and crystalline bending deformation of terminal carbon of hydrocarbon chain[16,72,80]. These modes can be further subdivided by the commonly identified factor group splitting seen in vibrational spectroscopy, where the peaks forming the doublet can be expressed as combination of other vibrational modes[85,86,87]. The orthorhombic crystalline phase spectral vibration (identified as B_{3U} (T_x)), in Figure 2.4 A, is characteristic of a skeletal vibration which is occurs between chains located in the lattice at 1471 cm^{-1} [86]. The crystal packing allows for the hydrocarbon chains to maintain a

symmetric and low energy state, requiring a higher frequency of energy to cause molecular vibrations. The gauche disordered phase (identified as B_{1G} (σ)), Figure 2.4 B, has a unique internal hydrogen vibration characteristic to this phase[86]. The vibrational mode seen in Figure 2.4 B can be divided into components producing signals at 1461 and 1457 cm^{-1}, therefore combining the intensities of these peaks account for the total intensity of the amorphous fraction.

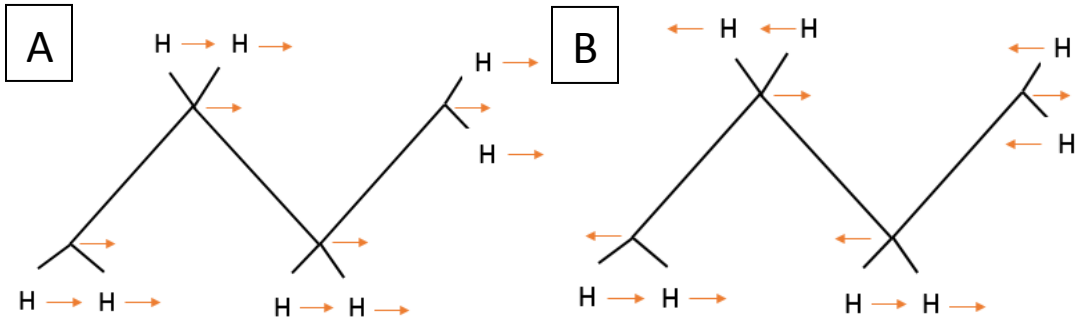

Figure 2.4: The vibrational modes of the crystalline B_{3U} (T_x), panel A, and amorphous B_{1G} (σ), vibrational modes of polyethylene, panel B. The amorphous vibrational mode produces two resonant peaks which give the net intensity when combined.

The FTIR spectra of the characteristic crystalline region in polyethylene is seen in Figure 2.5. The most noticeable change is between the control sample (black) and the aged samples, where the large crystalline peak with a shoulder transforms into a doublet with a slightly larger amorphous peak accompanied by a broad shoulder (A_g vibrational mode resonance peak)[87]. This indicates an increase in the amorphous content, but the magnitude of the crystalline peak appears to remain unchanged.

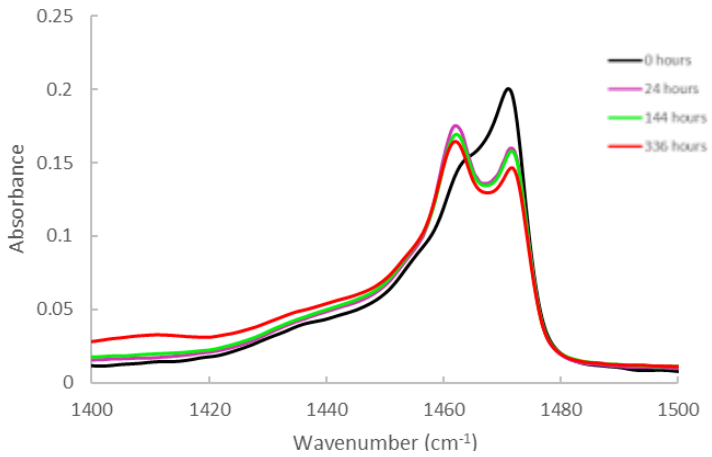

Figure 2.5: Expansion of FTIR spectra in the crystalline characterization regions of polyethylene after indicated aging period at 110℃. Each spectrum is an average of 3 scans.

Figure 2.6 shows the results of the surface crystallinity produced from the FTIR spectra and Equation 4. The results indicate an initial crystallinity of 53.8%, consistent with the manufacturing specifications of around 50%[18]. An initial increase in crystallinity, followed by a period of decrease and subsequent increase is apparent. This trend is consistent with similar techniques used on HDPE[33].

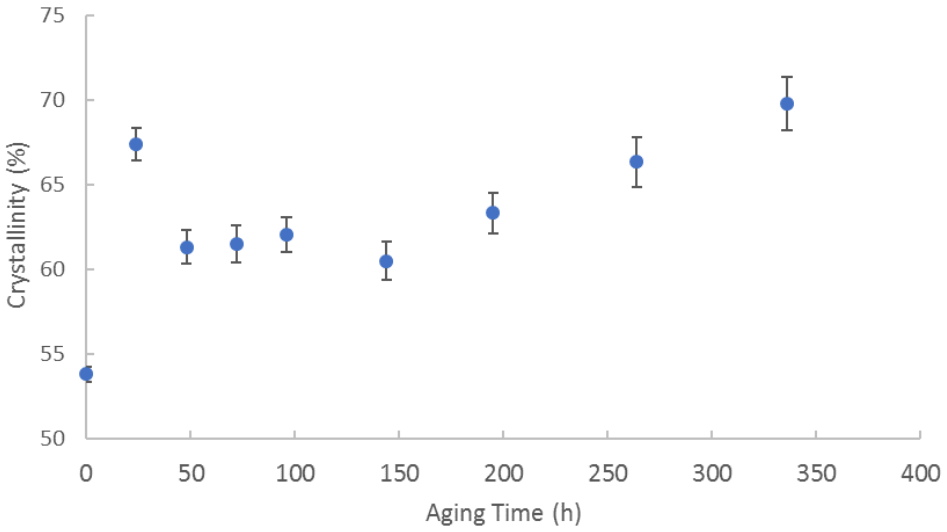

Figure 2.6: The average crystallinity of polyethylene after the indicated aging period at 110°C. Each point represents the average of 9 spectra and error bars represented as the standard deviation of each point.

These results suggest a three-phase physical process which consists of an initial annealing period followed by lattice breakdown and finally fragment packing which leads to the slow crystallinity increase. We attribute initial thermally-induced increase in crystallinity to annealing, which is hypothesized to be due to release of the internal conformational stress created within the polyethylene during the cooling process after production of the film[88]. Thermally-induced energy allows the strained, *gauche*, conformation to rotate into a favored *trans* position and participate in crystal structure[89,90]. Whether these *gauche* transformations are happening within the amorphous area, along the edge of the crystalline region or within the crystalline lamellae is currently unknown. Other reported phenomena known as an (alpha)- relaxation process may also be occurring, where

rearrangement of chains draws terminal carbons into the lamellae, and rotates to reduce strain on chain branches, thus increasing crystalline character[63]. This increased crystallinity period, however, was not observed at aging temperatures of 120°C, which we attribute to a complete loss of crystallinity due to melting of the samples (See Appendix for crystallinity analysis of samples thermally aged at 120°C).

Upon annealing, Figure 2.6 shows a decrease in crystallinity from 48 h to 144 h aging that is not typically observed. This makes the apparent period of decreased crystallinity an unexpected result. Pristine blown polyethylene films have shown to have surface peroxide content because of the manufacturing process[45,61]. One hypothesis is that chemical crosslinking between peroxides and neighboring chains, increasing the number of crosslinks[45]. These locations may serve as a tether between two large chains, causing temporary *gauche* deformations.

The increasing crystallinity in the later timepoints of aging can be attributed to the decreasing molecular where weight hydrocarbon chains undergo random scission, the efficiency of orthogonal packing increases in the *trans* conformation[89]. Chain scission is also accompanied by crosslinking, which is also suggested by a decrease in elastic modulus, but increase in hardness, proposing a decrease in chain length while increasing asymmetry of the lattice[32].

2.2.4 ATR-FTIR Crystallinity Method Evaluation and Validation

The IR band fit method for determining crystallinity with Omnic was evaluated for error and compared to another band fitting software method to validate the crystallinity calculation. The 3-stage crystallinity change observed in the IR spectra and shown in figure 2.6 was predicted based off literature review of how polymer morphology changes upon aging. The standard deviations of these measurements were maximally 3%, which suggests a promising quantification method. To ensure the observed trend was not the result of sample biasing, all spectra for samples (81 total) were collected and analyzed, which include normalizing, plotting and interpreting.

Some challenges with the Omnic method included analysis of noisy spectra, which sometimes varied crystallinity by 15-25% from the average. It was obvious these spectra were not representative, as the peak finding feature revealed up to 12 peaks, instead of the 4 known by literature[74–76]. Although manufacturer specifications indicate background stability for up to 120 minutes, the noisy spectra were attributed to backgrounds older than 10 minutes. To overcome the error from the noise, sample spectra were re-collected to produce a less noisy data set. Since the software allows the user to determine the number of times the fitting iterations are run, it is possible to vary the crystallinity by 1-2%, however, a two-tailed T-test indicated no difference between the maximum and minimum crystallinity values attained in a single spectrum. The sensitivity and noise target of the fitting was optimized empirically and were chosen when the spectral bands the software fit corresponded to literature to support IR vibrations[74–76].

To compare the abilities of the Omnic software with a separate peak-fitting program, IGOR Pro Multi-peak fit was used, alongside the formula for determining crystallinity. We determined the method did not meet the statistical rigor needed because the standard deviations were over 10%. The high error of the Igor fitting program likely results because the program's inflexibility in adjusting the sensitivity and noise targets

2.2.5 Evaluating Crystallinity with Differential Scanning Calorimetry

DSC is a common thermal method for evaluating the crystallinity of a polymer sample[31,91,92]. These measurements give a crystallinity measurement of the bulk sample. As is customary in DSC measurements, the thermogram was collected with an initial heating cycle, giving information about the thermal history of the polymer such as differences in thermal exposure, or VOC among samples. Figure 2.7 shows the heat flow from polymers on the first heat cycle. While there are many differences between the appearance of the 1st cycle data, there is no obvious trend with the varied aging times. One conclusion that can be made, however, is that the most aged sample (336 h) has a noticeably narrower melting peak. This may be the result of a more homogenized crystallinity because the packing of small molecular weight bands causes less varied thermal history. This first heating cycle can unfortunately not be used for quantitative determination of bulk crystallinity because the constraints of the sample pan and the morphology of the thin films does not allow for homogenous contact with the sample pan. Therefore, the 1st heating cycle seen in Figure 2.7 additionally serves as a sample

preparation step to ensure the polymer is in contact with the base of the pan where the heat flow is measured.

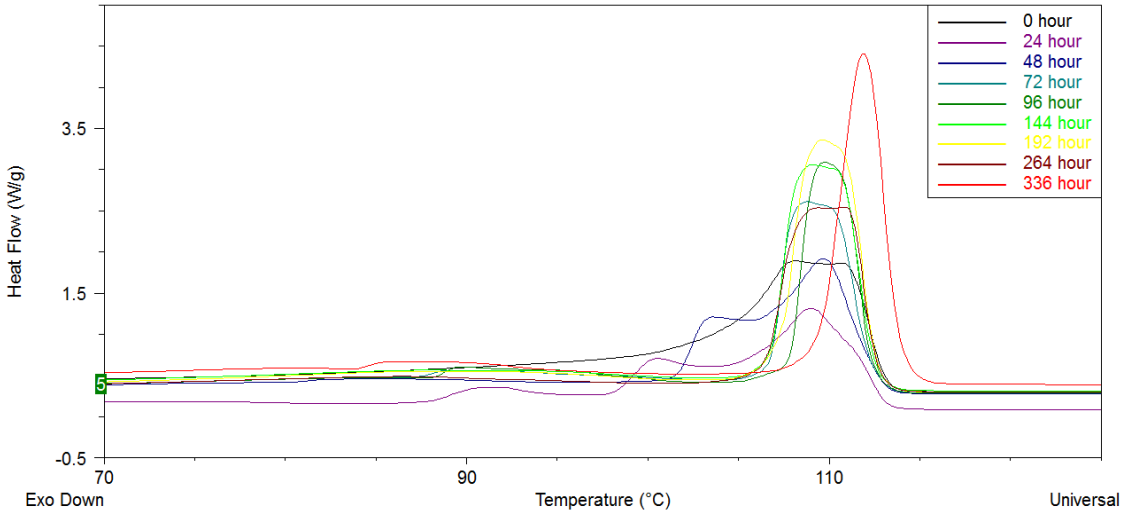

Figure 2.7: Heating cycle 1 before removal of thermal history.

Quantitative measure of crystallinity is obtained from the crystallization and cooling cycle, 3. This cycle is collected after a second heating cycle, 2. Figure 2.8 shows a heat flow diagram produced by DSC indicating the changes in heat flow from the sample during melting and crystallization. The measurement follows a heating curve from top left to right, then a cooling curve from bottom right to left. The endothermic, upward heating peak indicates the energy flux into the sample pan as it tries to maintain the same temperature as the reference pan, and in reverse with the exothermic, downward cooling peak.

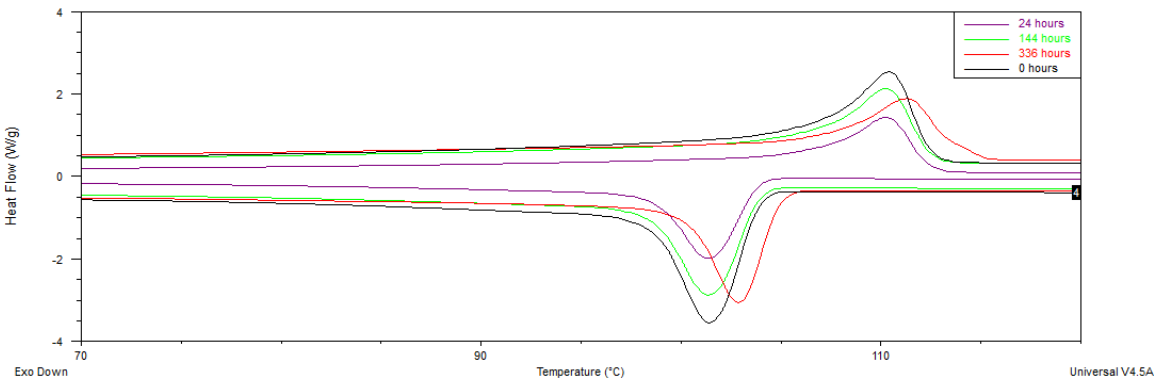

Figure 2.8: DSC heat flow of polyethylene after indicated aging period at 110℃. Heating cycle 2 and cooling cycle 3 are shown using representative spectra.

Figure 2.9 is the DSC determination for the crystallinity using the cooling peak. A distinct drop in crystallinity from the pristine sample is followed by a slight recovery and then plateau in crystallinity. Due to time constraints, samples were not collected in triplicate and so statistical analysis could not be performed.

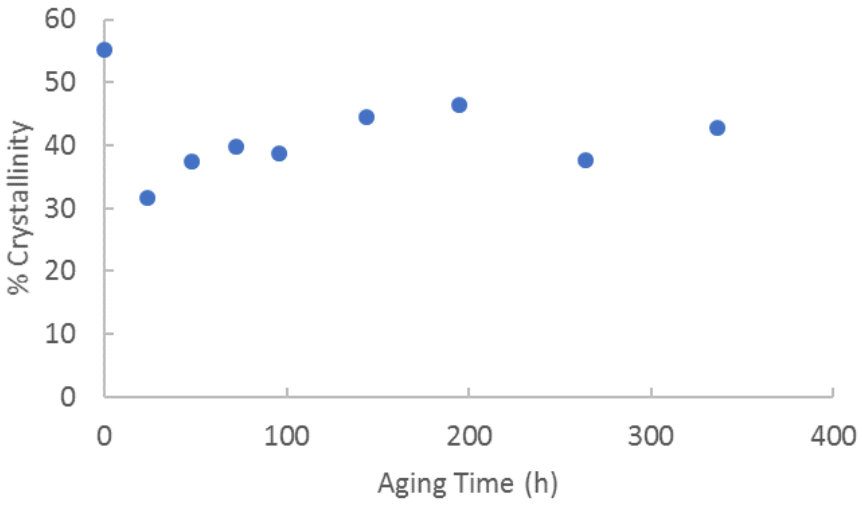

Figure 2.9: Crystallinity values determined by DSC for polyethylene aged at 110°C. These were not performed in triplicate due to time constraints

Since DSC measures the heat flow of the entire sample, it is a bulk measurement, rather than a surface measurement like ATR-FTIR, where < 1 μm of the surface of the material is measured. An initial decrease in crystallinity, followed by an insignificant change in crystallinity for samples aged over 400 hours. Although the decrease in crystallinity from the pristine polymer is not a reported consistently within the literature, simulations report a period of undisturbed crystallinity change, followed by a gradual increase under similar thermal conditions[93]. An explanation for our results suggests chain scission reactions have not occurred homogeneously through the polymer which is a main contributor to increasing crystallinity. Another explanation for the variability in the FTIR and DSC results is that the 1st melting cycle performed on DSC erased any of the non-chemical changes to the polymer crystallinity, which were preserved in the IR measurements. Figure 2.10 shows the comparison of crystallinity measurements from both FTIR and DSC. These techniques agree between the pristine samples (within 2%), which suggests initial crystalline homogeneity. Since these measurements only represent 1 sample at each aging time point, further insight into the bulk crystallinity will require replicate measurements.

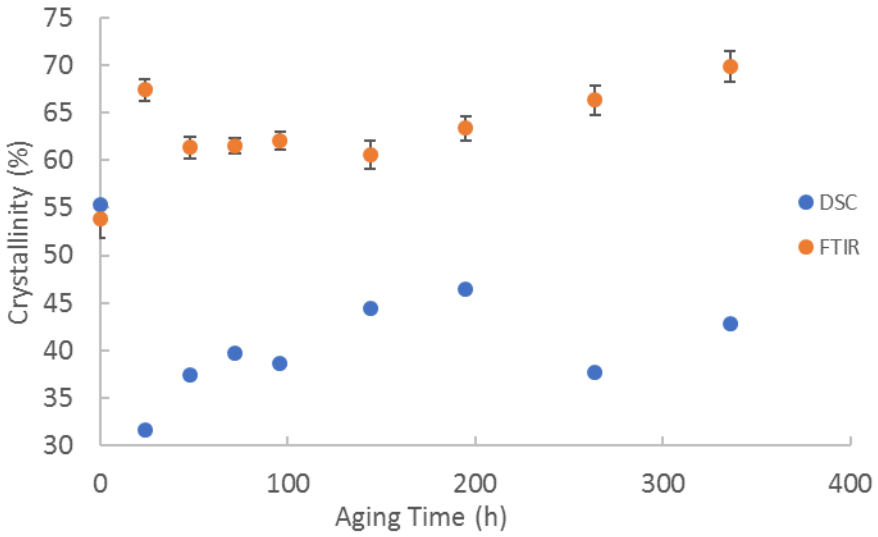

Figure 2.10: Comparison of crystallinity measurements made by DSC and FTIR.

The polyethylene aging study has shown that extended thermal exposure to films inflicts both chemical and physical changes. To further support the aging timeline put forth in Figure 1.7, direct studying of the aged polyethylene barrier properties was performed using electrical impedance spectroscopy.

2.2.6 Electrical impedance spectroscopy

Electrical impedance spectroscopy (EIS) is a technique that can be used to test properties of barriers, among other applications[94–96]. Resistivity, dielectric constant and diffusivity can be determined by producing an electrical current in response to an applied voltage to explain chemical phenomena. Two electrodes in solutions, separated by the barrier being studied, have a small AC electric potential applied across the system in addition to a DC voltage. If ions exist in the solution, the DC potential can be used to drive them in the direction of the potential. Based on how these ions interact with the barrier (act as a

capacitor, resistor or permeable membrane), the electrical signal output can be interpreted in a Bode or Nyquist plot. The Bode plot indicates the frequency-dependent impedance of the barrier in a log frequency-log modulus of impedance plot, and the Nyquist log (real impedance)- log (imaginary impedance) gives insight about the processes at play at the barrier.

In our study, we use a solution of citrate-capped gold nanoparticles, and one of double-distilled water (18 MΩ), separated by the polyethylene film to be studied. We employ an AC voltage across the cell to drive the nanoparticles into the film to act as stabilizers for the formed pores. The gold chloride pre-cursor was also used instead of gold nanoparticles, in case this was not completely removed during cleaning. The changing impedance of the barrier upon exposure to the solutions may also indicate breakdown in the barrier properties of the film.

336-hour aging with gold nanoparticles

Several measurements were taken under varying EIS conditions using the sample aged for 336 hours. The sample showed the greatest magnitude of aging, as both the high crystallinity and carbonyl index indicates extensive molecular scission that would allow for the deepest penetration of nanoparticles into the surface. Unfortunately, the oven aging process caused two of the three samples aged for 336 hours to fuse together, leaving only one sample for measurements.

The nanoparticle solutions prepared in the earlier section were used in the cells (denoted as AuNP), with the counter solution being MilliQ double distilled water (denoted as MQ). Figure 2.11 shows the Bode plot produced. The MQ/MQ Control sample (black) of

pristine polyethylene with no treatment. This is the only sample with double distilled water on both cell halves. No apparent loss of impedance at low frequency was observed.

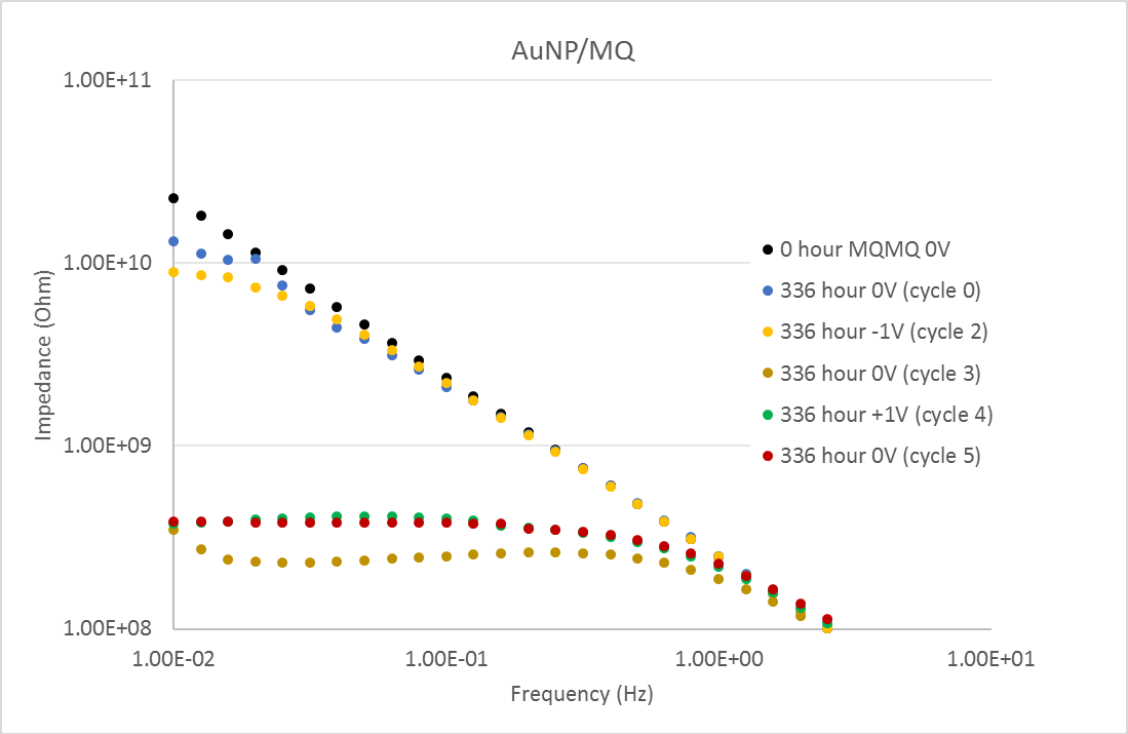

Figure 2.11: The Bode plot produced when the polyethylene aged at 110°C for 336 hours is placed in the cell. The cells contain gold nanoparticle solution and MQ respectively. Only the low-frequency portion of the spectra is shown.

Initially, there is an apparent decrease in the impedance of the aged polyethylene sample before any voltage is applied, suggesting thermal aging of the film has caused it to deteriorate as a barrier (Figure 2.11, blue). After applying a voltage of -1, the impedance drops more, suggesting the nanoparticles are decreasing the barrier properties of the film (Figure 2.11, gold). At this point, the film was flipped in the cell, exposing the film side potentially containing nanoparticles away from the electrolyte solution (Figure 2.11, bronze). The overall impedance shows a dramatic decrease, as well as a decreasing

component at low frequencies, that may be nanoparticles being driven out of the film and into the MilliQ water side. After this, a slight recovery in impedance is seen which may be attributed to the saturation of the film with water (Figure 2.11, green and red).

Another key piece of information gathered from the cycle measurements is the Nyquist plot, which provides insight to possible transport mechanisms occurring at the polymer interface. Cycle 3 may have suggested diffusion of nanoparticles from the polymer surface, and after analysis of the Nyquist plot, preliminary attempts at modelling an equivalent circuit were made (Figure 2.12) and values assigned in Table 2.2.

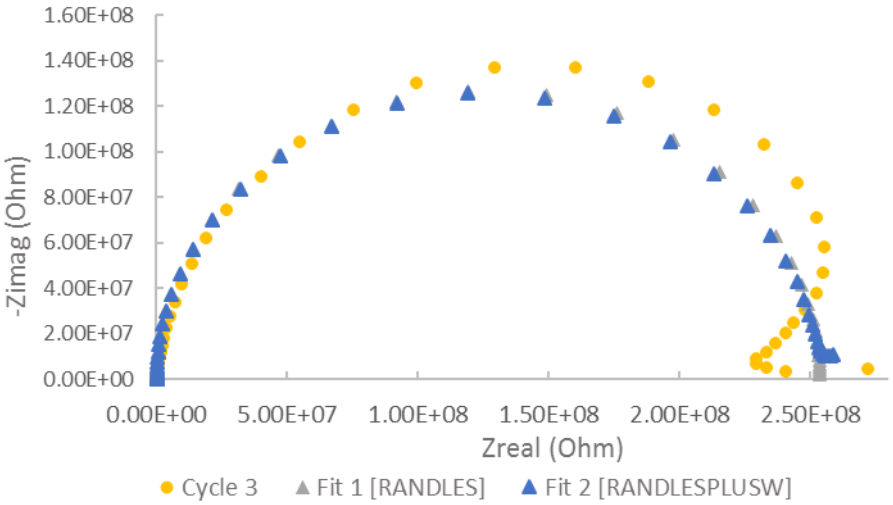

Figure 2.12: The Nyquist plot of Cycle 3 AuNP/MQ EIS results, overlaid with a simple Randles model and Randles model with a Warburg impedance factor.

Table 2.2: Fit values of the models produced for Cycle 3 of AuNP/MQ EIS results

Fit	Variable	Value	Uncertainty	Units
Randles	Rs	2.54E+08	1.36E+06	ohms
	Rct	8.88E+04	740.5	ohms
	Cf	5.27E-10	2.34E-12	F
	Goodness of Fit	1.20E-01		
Randles plus Warburg	Rs	2.50E+08	1.88E+06	ohm
	Rct	8.88E+04	8.26E+02	ohm
	Cf	5.26E-10	2.61E-12	F
	Warburg	3.33E-07	1.13E-07	$S*s^{(1/2)}$
	Goodness of Fit	1.20E-01		

Fitting to both a simple Randles circuit and Randles with a Warburg impedance factor yielded similar results, however further modelling is needed to produce a more accurate representation. Corrosion was seen on the alligator clips prior to use (unrelated to this experiment), which may have also influenced the resistivity of the system, possibly having an effect during the modelling.

264-hour aging with gold chloride

The nanoparticle pre-cursor $HAuCl_4$ was also tested as an electrolyte solution in the EIS to see the effects of chloride and gold ions on the aged film. We have seen evidence of chloride and gold ions influencing impedance with thermally aged polyethylene films (See Appendix). A negative potential will drive chloride ions towards the film, and gold with a positive potential. Due to a lack of samples available, only one film aged for 264 hours was tested. Figure 2.13 shows the Bode plot for these samples. The MQ/MQ Control sample of pristine polyethylene with no treatment. This is the only sample with

double distilled water on both cell halves. No apparent loss of impedance at low frequency.

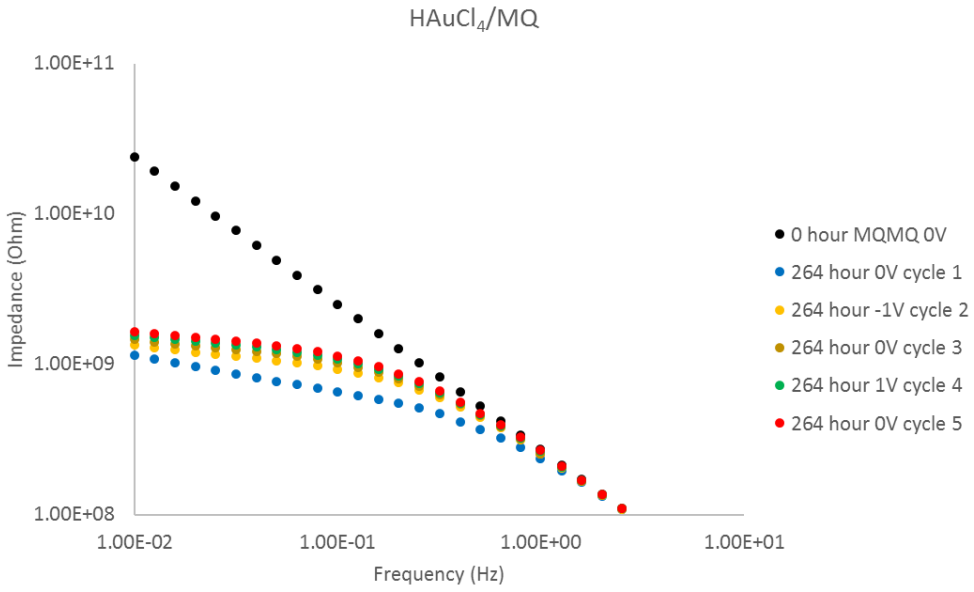

Figure 2.13: The Bode plot produced when the polyethylene aged at 110°C for 264 hours is placed in the cell. The cells contain $HAuCl_4$ solution and MQ respectively. Only the low-frequency portion of the spectra is shown.

The film shows an initial decrease in impedance, followed by a gradual recovery independent of the potential. The decrease may either be from the aging process, or from the electrolyte solution. This general upward trend in impedance has been seen in previous measurements I have made. This may be attributed with increasing water-volume fraction within the polymer which would increase resistivity. There appears to be no effect on the film impedance provided by the applied voltage. This could suggest pores which allow ions to freely flow between them.

A corresponding Nyquist plot was collected for the representative spectrum of Cycle 1 to identify a Warburg element which may suggest ion flow (Figure 2.14).

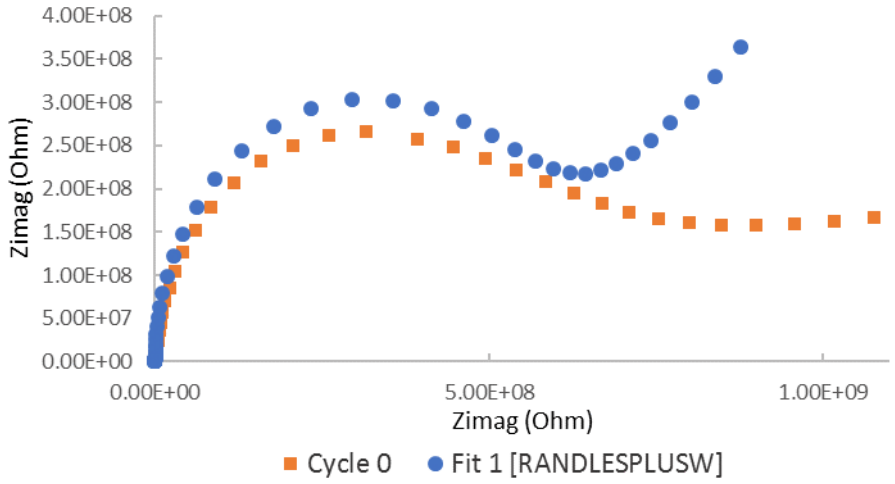

Figure 2.14: The Nyquist plot of Cycle 0 $HAuCl_4$/MQ EIS results, overlaid with a Randles model and a Warburg impedance factor.

The modelling results seen in Table 2.3 suggest a Warburg element which provides support for the idea that ions may be exchanging through the polyethylene film. Further analysis will need to be performed to get a better understanding of the factors playing into the model.

Table 2.3: Fit values of the models produced for Cycle 0 of $HAuCl_4$/MQ EIS results

Fit	Variable	Value	Uncertainty	Units
Randles plus Warburg	Rs	5.54E+08	6.00E+06	ohm
	Rct	7.55E+04	6.65E+02	ohm
	Cf	4.94E-10	2.26E-12	F
	Warburg	8.23E-09	2.57E-10	S*s^(1/2)
	Goodness of Fit	8.48E-02		

A complimentary method to identifying both if pores are present and if they can be saturated with nanoparticles could be done through SEM imaging of the films. Specifically, the use of EDX (energy dispersive x-ray) analysis can identify different elements within the film.

2.2.7 Scanning electron microscopy (SEM)

To better compliment the results from the EIS measurements, SEM imaging was performed on the films and electrodes to find the presence of ions either embedded in the film, or the electrodes of the cell. Secondary electron imaging was performed to assess the quality of the film surface. Backscattered electron imaging in a topographic mode gave insight into the roughness of the film surface before and after aging, and the elemental mode showed the presence of ions which may have been sorbed during the EIS measurements.

Since carbon coating would mask the detection of gold, or chloride embedded in the film, it was not done in preparing the samples. This, however, means charging on the surface was a major issue when working with polyethylene. Two methods employed to help reduce charging were decreasing accelerating voltage, or imaging in a low-vacuum mode (≈15 Torr). Decreasing accelerating voltage showed reduced charging, but with decreased image resolution. Low vacuum also reduced charging, but similarly decreased resolution and did not allow for accurate elemental analysis.

Figure 2.15 reveals morphological changes to polyethylene after thermal aging at 78°C for 10 days. Areas appearing light indicate a higher location on the polymer, as opposed to depressions shown as darker. The pristine polymer shown in Figure 2.15 A indicates a very smooth, homogeneous surface with two long abrasions running top left to bottom right. These were most likely caused from handling the plastic, as they do not penetrate deep into the polymer. Figure 2.15 B shows long vertical lines running down the polymer, as well as some from top left to bottom right. These are indications of slight differences in polymer surface depth, most likely caused from polymer thickening known to occur at elevated temperature.

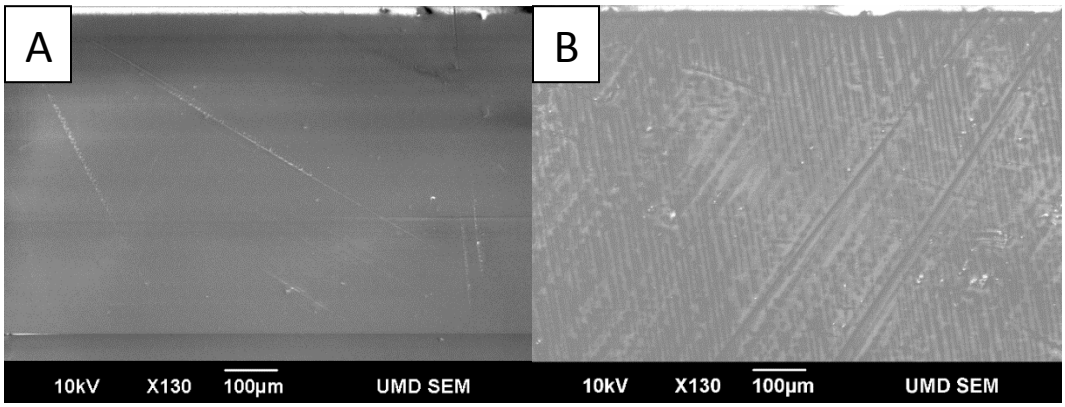

Figure 2.15: SEM-BE topography imaging of pristine polyethylene (A) and thermally treated polyethylene at 78°C for 10 days (B). Accelerating voltage of 25 kV.

Elemental Analysis

To identify the species within the film, backscattered electron imaging is used. The electrons emitted from the microscope hit the sample and are elastically scattered back

towards the detector. Since heavier elements, such as gold, scatter more strongly than lighter elements, such as carbon, the signal produced is stronger and appears brighter in images. Figure 2.16 shows a SEM-EDS compo image of gold nanoparticle concentrate on polyethylene, where nanoparticle clusters appear as bright areas. Clustering is an effect of the drying process on top of the film.

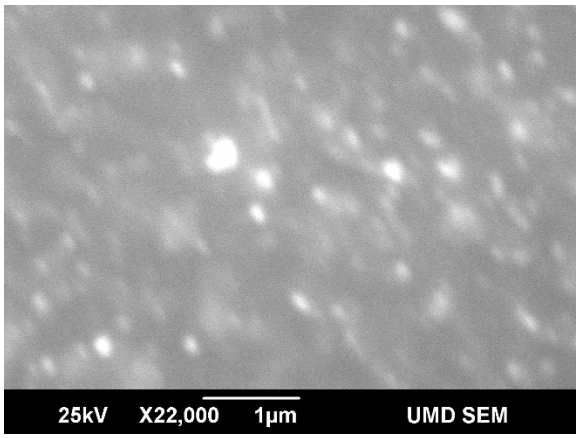

Figure 2.16: Gold nanoparticles (white) on polyethylene. Accelerating voltage of 25 kV.

If the decrease in impedance indicated by the EIS in both the 264 and 336 hour samples is due to permeation with nanoparticles or $HAuCl_4$ ions, we hope to identify these chemicals on either the electrode opposite the electrolyte solution, or within the film itself. Images provided are for spectral purposes only. Significant charging on the surface can be seen in the form of vertical, lightening-like lines. The color gradient is caused by the scan rate of the detector as it surveys the surface.

The results for the elemental composition of the spectral region analyzed is outlined in Table 2.4. One spectrum from each elemental analysis is presented. EDS images indicating spectral location can be found in the Appendix.

Table 2.4: Elemental analysis results for aged polyethylene after cycling in the EIS cell from Figure 2.10 and Figure 2.12.

Spectrum	C	O	Si	Cl	Au	Total
336 AuNP side*	93.65	5.93	0.41			100.00
336 MQ side	94.42	5.26	0.32			100.00
336 MQ electrode	94.69	5.31				100.00
264 MQ side	93.81	5.51	0.63	0.05		100.00
264 $HAuCl_4$ side	95.45	3.72			0.83	100.00
264 MQ electrode	100.0					100.00

All results in weight%
*The side facing the nanoparticle solution, after the rotation

The results indicate no presence of gold either in the film or on the counter electrode of the EIS cell for polyethylene aged for 336 hours, however silicon is present. The lack of gold present may be due to very low concentrations, causing the signal to be below detectable limits set for INCA software. A limitation of the SEM used was a complete loss of lateral resolution below 100 nm, which is 10 × lower than the size of a single nanoparticle and may also explain the inability to locate nanoparticles when surveying the surface. The presence of silicon can be explained by the rubber stoppers used to cover and hold the electrode in each cell. Condensation formed on the bottom of the stopper was noted after the EIS analysis. The presence of oxygen on the film also indicates

oxidation, which is supported by the carbonyl indexing. Oxygen may also be present even in high vacuum mode.

Elemental analysis for the EIS cell of polyethylene aged for 264 hours reveals several ions indicative of diffusion through the film. Although no gold or chloride appear to be on the counter electrode, presence of both are seen on the film. The nanoparticle-facing side of the film indicates presence of gold embedded in the surface, and the presence of chloride on the opposing side. This suggests diffusion of chloride through the film, which is consistent with the reading indicated by the EIS.

Although it would be beneficial to further investigate the relative abundance of elements detected, I realized several ambiguities with the method that the elemental analysis produces the values. The rate of electron backscatter from an element is proportional to which signal it is producing (Kα, Lα or Mα line). The line produced from carbon requires significantly less energy to produce a signal (Kα 0.277 keV) as opposed to that of gold (Mα 2.123 keV). Therefore, the ratio of carbon to gold signal is not equivalent. It is also unclear how the software calculates an abundance from a signal count. Further investigation is needed before a reasonably explainable quantitative analysis should be performed.

Combining the results of both the EIS and elemental analysis, we show support for several conclusions about the breakdown of polyethylene films. There appears to be a decrease in the impedance of the film after 336 hours of thermal aging. Upon exposure to nanoparticles, there is a significant decrease in impedance, however elemental analysis results do not indicate the presence of nanoparticles. In contrast, the 264 hour samples

both indicate a drop in impedance upon exposure, and presence of gold and chloride ions embedded in the film. This may suggest the formation of pores large enough to accommodate select ions. The hydrated radius of the chloride ion has been calculated to be between 0.27 – 0.29 nm[97], in comparison to the ≈ 5 – 10 nm gold nanoparticles (no reported hydrated radius of gold). This gives a general estimate of a pore size of at least 0.3 nm consistent through the film.

2.3 Conclusions

A predictive aging model for low density polyethylene insulative cable housings was developed. This model revealed a combination of physical and chemical processes which lead to an increase in permeability and decrease in strength of the insulator. In creating this predictive model, a gap of knowledge in the literature was revealed in two areas: understanding how the crystallinity of a polymer changes with time, and visualizing the predicted pores formed through the insulator which leads to failure.

While measuring crystallinity of semi-crystalline polyethylene is not a novel idea, monitoring it as an aging indicator under thermally oxidative conditions has not been reported. Developing and using an adapted ATR-FTIR method, crystallinity was monitored over 336 hours and a three-phase aging timeline. To compliment this, DSC was performed to assess bulk crystallinity but revealed inhomogeneity in crystallinity changes. Other peak fitting software was also used to test the consistency of the FTIR method but was found to be less reliable.

To visualize pore structure and test barrier properties, EIS was used to saturate these aged polyethylene films with synthesized citrate-capped gold nanoparticles, and

chloroauric acid precursor. The results indicate a decreasing impedance of the polyethylene films caused by the transport of ions through the film. SEM imaging was then performed for elemental analysis of the films and counter electrodes for the presence of ions. Chloride and gold ions were detected; however, no nanoparticles were found. This gives an estimated pore size of at least 0.3 nm through the aged film.

To elucidate pore structure, we will be using TEM to image the films saturated with nanoparticles in the hopes of identifying locations of penetration through the surface. This could be then used to generate a 3D image of the structure of the pore.

References

1. Skrovanek, D. J., Painter, P. C. & Coleman, M. M. Hydrogen Bonding in Polymers. 2. Infrared Temperature Studies of Nylon 11. *Macromolecules* **19**, 699–705 (1986).

2. Murthy, N. S., Minor, H., Bednarczyk, C. & Krimm, S. Structure of the Amorphous Phase in Oriented Polymers. *Macromolecules* **26**, 1712–1721 (1993).

3. Messori, M. *et al.* Prevention of plasticizer leaching from PVC medical devices by using organic-inorganic hybrid coatings. *Polymer (Guildf).* **45**, 805–813 (2004).

4. *Medium Voltage Underground Cable White Paper*. (2006).

5. Brown, J. *et al.* SANDIA REPORT Submerged Medium Voltage Cable Systems at Nuclear Power Plants : A Review of Research Efforts Relevant to Aging Mechanisms and Condition Monitoring Org 1835 : Organic Materials Science. (2015).

6. Tamboli, S. M., Mhaske, S. T. & Kale, D. D. Crosslinked polyethylene. *Indian J. Chem. Technol.* **11**, 853–864 (2004).

7. Hinderliter, B. R., Croll, S. G., Tallman, D. E., Su, Q. & Bierwagen, G. P. Interpretation of EIS data from accelerated exposure of coated metals based on modeling of coating physical properties. *Electrochim. Acta* **51**, 4505–4515 (2006).

8. Barone, V. *et al.* Role and Effective Treatment of Dispersive Forces in Materials : Polyethylene and Graphite Crystals as Test Cases. (2008). doi:10.1002/jcc

9. Reano, A. F., Guinault, A., Richaud, E. & Fayolle, B. Polyethylene loss of ductility during oxidation: Effect of initial molar mass distribution. *Polym. Degrad. Stab.* **149**, 78–84 (2018).

10. Lu, X. & Brown, N. Effect of thermal history on the initiation of slow crack growth in linear polyethylene. *Polymer (Guildf).* **28**, 1505–1511 (1987).

11. Boukezzi, L. & Boubakeur, A. Oxidation Evaluation of Cross-linked Polyethylene (XLPE) under Thermal Degradation : FTIR Study. (2010).

12. Boukezzi, L. Prediction of Mechanical Properties of XLPE Cable Insulation Under Thermal Aging : Neural Network Approach. *IEEE Trans. Dielectr. Electr. Insul.* **20**, 2125–2134 (2013).

13. Strobl, G. R., Schneider, M. J. & Voigt-Martin, I. G. Model of partial crystallization and melting derived from small-angle X-ray scattering and electron microscopic studies on low-density polyethylene. *J. Polym. Sci. Polym. Phys. Ed.* **18**, 1361–1381 (1980).

14. Tanabe, Y., Strobl, G. R. & Fischer, E. W. Surface melting in melt-crystallized linear polyethylene. *Polymer (Guildf).* (1986). doi:10.1016/0032-3861(86)90001-7

15. Sundararajan, P. R. & Kavassalis, T. A. Molecular Dynamics Study of Polyethylene Chain Folding : The Effects of Chain Length and the Torsional Barrier. **91**, 2541–2549 (1995).

16. Zhou, Y. *et al.* Confined crystallization and phase transition in semi-rigid chitosan containing long chain alkyl groups †. 561–567 (2011). doi:10.1039/c0ce00165a

17. Fischer, E. W. Small angle x-ray scattering studies of phase transitions in polymeric and oligomeric systems. *Pure Appl. Chem.* **26**, 385–421 (1971).

18. Goodfellow USA.

19. Thomas. Understanding Plastic Extrusion. *2019* Available at: https://www.thomasnet.com/articles/plastics-rubber/plastic-extrusions. (Accessed: 11th June 2019)

20. Paul, M. & Santosh, D. An approach to low-density polyethylene biodegradation by Bacillus amyloliquefaciens. 81–86 (2015). doi:10.1007/s13205-014-0205-1

21. Bogdal, D. Interaction of microwaves with different materials. in *Microwave-assisted Organic Synthesis* 1–11 (Elsevier, 2005).

22. Bent, H. A. Permeability to liquids of Polyethylene and Irradiated Polyethylene. *J. Polym. Sci.* **24**, 387–400 (1957).

23. Kamal, M. R. Permeability of Oxygen and Water Vapor Through Polyethylene / Pol yamide Films. *Soc. Plast. Eng.* **24**, 1340–1350 (1984).

24. Flaconnèche, B., Martin, J. & Klopffer, M. H. Permeability , Diffusion and Solubility of Gases in Polyethylene , Polyamide 11 and Poly (vinylidene fluoride). **56**, 261–278 (2001).

25. Karimi, M. Diffusion in Polymer Solids and Solutions. (2006).

26. Michaels, A. S. & Parker, R. B. J. Sorption and flow of gases in polyethylene. *J. Polym. Sci.* **41**, 53–71 (1959).

27. Siracusa, V. Food Packaging Permeability Behaviour: A Report. *Int. J. Polym. Sci.* **2012**, 1–11 (2012).

28. Matsuyama, H., Okafuji, H., Maki, T., Teramoto, M. & Kubota, N. Preparation of polyethylene hollow fiber membrane via thermally induced phase separation. *J. Memb. Sci.* **223**, 119–126 (2003).

29. Wang, M. *et al.* Investigation of water diffusion in low-density polyethylene by

attenuated total reflectance fourier transform infrared spectroscopy and two-dimensional correlation analysis. *Ind. Eng. Chem. Res.* **50**, 6447–6454 (2011).

30. Weon, J. Il. Effects of thermal ageing on mechanical and thermal behaviors of linear low density polyethylene pipe. *Polym. Degrad. Stab.* **95**, 14–20 (2010).

31. Grabmayer, K. *et al.* Accelerated aging of polyethylene materials at high oxygen pressure characterized by photoluminescence spectroscopy and established aging characterization methods. *Polym. Degrad. Stab.* **109**, 40–49 (2014).

32. Andrady, A. L., Pegram, J. E. & Tropsha, Y. Changes in carbonyl index and average molecular weight on embrittlement of enhanced-photodegradable polyethylenes. *J. Environ. Polym. Degrad.* **1**, 171–179 (1993).

33. Fejdyś, M. & Łandwijt, M. Effect of Accelerated Ageing Conditions on the Degradation Process of Dyneema® Polyethylene Composites — Fibres & Textiles in Eastern Europe. **19**, 60–65 (2011).

34. Bhateja, S. K. Changes in the crystalline content of irradiated linear polyethylenes upon ageing. *Polymer (Guildf).* **23**, 654–655 (1982).

35. Minor, H. & Technology, C. General procedure for evaluating amorphous scattering and crystallinity from X-ray diffraction scans of semicrystalline polymers. *Polymer (Guildf).* **31**, 996–1002 (1989).

36. Tung, B. L. H. THE EFFECT OF MOLECULAR WEIGHT ON THE CRYSTALLINITY OF POLYETHYLENE1. **495**, 1530–1534 (1957).

37. Bowler, N. & Liu, S. Aging Mechanisms and Monitoring of Cable Polymers. *Progn. Heal. Manag. Soc.* 1–12 (2015).

38. Jeon, H. J. & Kim, M. N. Degradation of linear low density polyethylene (LLDPE) exposed to UV-irradiation. *Eur. Polym. J.* **52**, 146–153 (2014).

39. Sugimoto, M., Shimada, A., Kudoh, H., Tamura, K. & Seguchi, T. Product analysis for polyethylene degradation by radiation and thermal ageing. *Radiat. Phys. Chem.* **82**, 69–73 (2013).

40. Balasubramanian, S. K., Yang, L., Yung, L. L., Ong, C. & Ong, W. Biomaterials Characterization , puri fi cation , and stability of gold nanoparticles. **31**, 9023–9030 (2010).

41. Oluwoye, I., Altarawneh, M., Gore, J. & Dlugogorski, B. Z. Oxidation of crystalline polyethylene. *Combust. Flame* **162**, 3681–3690 (2015).

42. Day, M. & Wiles, D. M. Photochemical Degradation of Poly (ethylene Terephthalate). II . Effect of Wavelength and Environment on the Decomposition Process. *J. Appl. Polym. Sci.* **16**, 191–202 (1972).

43. Day, M. & Wiles, D. M. Photochemical Degradation of Poly(ethylene Terephthalate) . III. Determination of Decomposition Products and Reaction Mechanism. *J. Polym. Sci.* **16**, 203–215 (1972).

44. Toop, D. J. Theory of Life Testing and Use of Thermogravimetric Analysis to Predict the Thermal Life of Wire Enamels. *IEEE Trans. Electr. Insul.* **EI-6**, 2–14 (1971).

45. Gugumus, F. Re-examination of the role of hydroperoxides in polyethylene and polypropylene: chemical and physical aspects of hydroperoxides in polyethylene. *Polym. Degrad. Stab.* **49**, 29–50 (1995).

46. Seguchi, T., Tamura, K., Ohshima, T., Shimada, A. & Kudoh, H. Degradation mechanisms of cable insulation materials during radiation–thermal ageing in radiation environment. *Radiat. Phys. Chem.* **80**, 268–273 (2011).

47. Shimada, A., Sugimoto, M., Kudoh, H., Tamura, K. & Seguchi, T. Degradation distribution in insulation materials of cables by accelerated thermal and radiation ageing. *IEEE Trans. Dielectr. Electr. Insul.* **20**, 2107–2116 (2013).

48. Richaud, E., Colin, X. & Fayolle, B. Induction Period in the Hydrocarbons: Oxidation of Saturated Low-Temperature Thermal Example of Polyethylene. *Int. J. Chem. Kinet.* **14**, 1–6 (2008).

49. Khelidj, N. *et al.* Oxidation of polyethylene under irradiation at low temperature and low dose rate. Part II. Low temperature thermal oxidation. *Polym. Degrad. Stab.* **91**, 1598–1605 (2006).

50. Reich, L. *Elements of Polymer Degradation*. (1971).

51. Aboulkas, A., El, K. & Bouadili, A. El. Thermal degradation behaviors of polyethylene and polypropylene . Part I : Pyrolysis kinetics and mechanisms. *Energy Convers. Manag.* **51**, 1363–1369 (2010).

52. Roy, P. K., Hakkarainen, M., Varma, I. K. & Albertsson, A. Degradable Polyethylene : Fantasy or Reality. 4217–4227 (2011). doi:10.1021/es104042f

53. Colin, X., Monchy-Leroy, C., Audouin, L. & Verdu, J. Lifetime prediction of polyethylene in nuclear plants. *Nucl. Instruments Methods Phys. Res. Sect. B Beam Interact. with Mater. Atoms* **265**, 251–255 (2007).

54. Zoltek, D. *et al.* CHARACTERIZING AND QUANTIFYING THE AGING OF POLYETHYLENE THIN FILMS USING NOVEL DOPED-FILMS AND GOLD NANOPARTICLE LABELING STRATEGIES. in (2019).

55. World Health Organization. Indoor air quality: organic pollutants. *EURO reports Stud. 111* (1987).

56. Bernstein, R. *et al.* The origins of volatile oxidation products in the thermal degradation of polypropylene, identified by selective isotopic labeling. *Polym. Degrad. Stab.* **92**, 2076–2094 (2007).

57. Atkinson, R. & Arey, J. Atmospheric Degradation of Volatile Organic Compounds. *Chem. Rev.* **103**, 4605–4638 (2003).

58. Contos, D. A. *et al.* Development of Emission Factors for Polyethylene Processing. *J. Air Waste Manag. Assoc.* **46**, 569–580 (1996).

59. Atkinson, R. Atmospheric chemistry of VOCs and NO(x). *Atmos. Environ.* (2000). doi:10.1016/S1352-2310(99)00460-4

60. Laurent, C., Mayoux, C. & Noel, S. Dielectric breakdown of polyethylene in divergent field: Role of dissolved gases and electroluminescence. *J. Appl. Phys.* **54**, 1532–1539 (1983).

61. Peterson, J. D., Vyazovkin, S. & Wight, C. A. Kinetics of the Thermal and Thermo-Oxidative Degradation of Polystyrene , Polyethylene and Poly (propylene). 775–784 (2001).

62. Mccaffrey, W. C., Kamal, M. R. & Cooper, D. G. Thermolysis of polyethylene. (1994).

63. Gedde, U. W. & Mattozzi, A. *Polyethylene Morphology. In: Albertsson AC. (eds) Long Term Properties of Polyolefins.* (Advances in Polymer Science, Springer).

64. Murthy, N. S., Akkapeddi, M. K. & Orts, W. J. Analysis of lamellar structure in semicrystalline polymers by studying the absorption of water and ethylene glycol in nylons using small-angle neutron scattering. *Macromolecules* **31**, 142–152 (1998).

65. Fischer, E. W. Neutron scattering studies on the crystallization of polymers. *Polym. J.* **17**, 307–320 (1985).

66. Schmidt-Rohr, K. & Spiess, H. W. Chain Diffusion between Crystalline and Amorphous Regions in Polyethylene Detected by 2D Exchange 13C NMR. *Macromolecules* **24**, 5288–5293 (1991).

67. O'leary, K. & Geil, P. H. Reversible Long-Period Changes During the Annealing of Crystalline Polymers. *Macromol. Sci.* **B1**, 147–160 (1967).

68. Boyd, R. H. Relaxation processes in crystalline polymers: experimental behaviour - a review. *Polymer* (1985). doi:10.1016/0032-3861(85)90192-2

69. Gheysari, D., Behjat, A. & Haji-Saeid, M. Effect of high-energy electron beam on mechanical and thermal properties of LDPE and HDPE. *Eur. Polym. J.* (2001). doi:10.1016/S0014-3057(00)00122-1

70. Clough, R. L. & Gillen, K. T. Oxygen diffusion effects in thermally aged elastomers. *Polym. Degrad. Stab.* **38**, 47–56 (1992).

71. Hui, Y. Thermogravimetry Study of the Thermal Stability and the Lifetime of High Density Polyethylene Film. 5–7 (2001).

72. Gulmine, J. V, Janissek, P. R., Heise, H. M. & Akcelrud, L. Degradation profile of polyethylene after artificial accelerated weathering. **79**, 385–397 (2003).

73. Peterlin, A. Chain Scission and Plastic Deformation in the Strained Crystalline Polymer. *J. Polym. Sci. Polym. Symp.* **32**, 297–317 (1971).

74. Painter, P. C., Havens, J., Hart, W. W. & Koenig, J. L. A Fourier Transform Infrared Spectroscopic Investigation of Polyethylene Single Crystals . I . Methylene Wagging Mode. *J. Polym. Sci.* **15**, 1223–1235 (1977).

75. Abbate, S., Gussoni, M. & Zerbi, G. Infrared and Raman intensities of polyethylene and perdeuteropolyethylene: Factor group splittings. *J. Chem. Phys.* **70**, 3577–3585 (1979).

76. Zerbi, G., Gallino, G., Del Fanti, N. & Baini, L. Structural depth profiling in polyethylene films by multiple internal reflection infra-red spectroscopy. *Polymer (Guildf).* **30**, 2324–2327 (1989).

77. Strobl, G. R. & Hagedorn, W. Raman spectroscopic method for determining the crystallinity of polyethylene. *Polym. Phys.* **16**, 1181–1193 (1978).

78. Hagemann, H. & Snyder, R. G. Quantitative Infrared Methods for the Measurement of Crystallinity and Its Temperature Dependence: Polyethylene. *Macromolecules* **22**, 3600–3606 (1989).

79. Strobl, G. R. & Hagedorn, W. Raman Spectroscopic Method for Determining the Crystallinity of Polyethylene. *J. Polym. Sci.* **16**, 1181–1193 (1978).

80. Gulmine, J. V, Janissek, P. R., Heise, H. M. & Akcelrud, L. Polyethylene characterization by FTIR. **21**, 557–563 (2002).

81. Piella, J. & Puntes, V. Size-controlled Synthesis of sub-10 nm Citrate-stabilized Gold Nanoparticles and Related Optical Properties . 1–10

82. Bast, N. G., Comenge, J. & Puntes, V. Kinetically Controlled Seeded Growth Synthesis of Citrate-Stabilized Gold Nanoparticles of up to 200 nm : Size Focusing versus Ostwald Ripening. 11098–11105 (2011). doi:10.1021/la201938u

83. Cytodiagnostics. Cytodiagnostics. (2019). Available at: http://www.cytodiagnostics.com/store/pc/viewcontent.asp?idpage=2. (Accessed: 11th June 2019)

84. Gamry instrument. Common Equivalent Circuit Models Part 3. *Gamry Instruments* **3**, 1–13 (2017).

85. Lagaron, J.-M. The Factor Group Splitting Phenomenon: A vibrational Spectroscopy Approach to Assess Polymer Crystallinity and Crystalline Density. *Macromol. Symp.* **184**, 19–36 (2002).

86. Krimm, S., Liang, C. Y. & Sutherland, G. B. B. M. Infrared spectra of high polymers. II. Polyethylene. *J. Chem. Phys.* **25**, 549–562 (1956).

87. Abbate, S., Zerbi, G. & Wunder, S. L. Fermi resonances and vibrational spectra of crystalline and amorphous polyethylene chains. *J. Phys. Chem.* **86**, 3140–3149 (1982).

88. Lin, J., Yan, W. & Tu, M. Crack initiation point determination and dynamic fracture toughness for Charpy pre-cracked specimen. *Acta Metall. Sin. Ser. A, Phys. Metall. Mater. Sci.* **5 A**, 379–384 (1992).

89. Shi, H., Zhao, Y., Jiang, S., Xin, J. H. & Rottstegge, J. Order e disorder transition in eicosylated polyethyleneimine comblike polymers. **48**, 2762–2767 (2007).

90. Ennis, C. P. & Kaiser, R. I. Mechanistical studies on the electron-induced degradation of polymers : polyethylene , polytetrafluoroethylene , and polystyrene. **12**, (2010).

91. Chen, Z. The Crystallization of Poly (ethylene terephthalate) Studied by Thermal Analysis and FTIR Spectroscopy. 219 (2012).

92. Colom, X. & Canavate, J. Changes in Crystallinity of the HDPE Matrix in Composites with Cellulose Fiber Using DSC and FTIR. *Reinf. Plast. Compos.* **19**, (2000).

93. Reano, A. F., Guinault, A., Richaud, E. & Fayolle, B. Polyethylene loss of ductility during oxidation: Effect of initial molar mass distribution. *Polym. Degrad. Stab.* **149**, 78–84 (2018).

94. Fernández-Sánchez, C., McNeil, C. J. & Rawson, K. Electrochemical impedance spectroscopy studies of polymer degradation: Application to biosensor development. *TrAC - Trends Anal. Chem.* **24**, 37–48 (2005).

95. Hinderliter, B. R., Croll, S. G., Tallman, D. E., Su, Q. & Bierwagen, G. P. Interpretation of EIS data from accelerated exposure of coated metals based on modeling of coating physical properties. *Electrochim. Acta* (2006). doi:10.1016/j.electacta.2005.12.047

96. Deflorian, F., Fedrizzi, L., Rossi, S. & Bonora, P. L. Organic coating capacitance measurement by EIS: Ideal and actual trends. *Electrochim. Acta* **44**, 4243–4249 (1999).

97. Tanganov, B. B. ABOUT SIZES OF THE HYDRATED SALT IONS – THE COMPONENTS OF SEA WATER. *Eur. J. Nat. Hist.* **1**, 36–37 (2013).

Appendix

The results of the gold nanoparticle synthesis yielded 4.9 ± 0.9 nm and TEM imaging was performed. The results are seen in Figure 1A

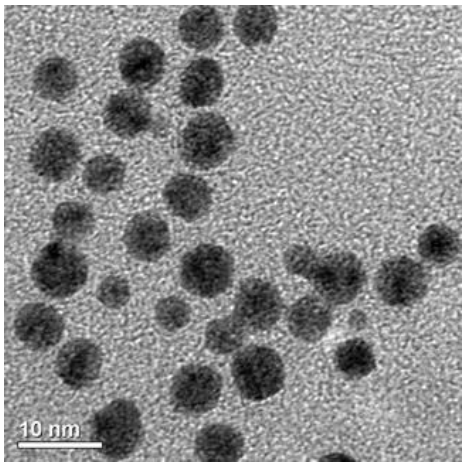

Figure A1: TEM image of gold nanoparticles.

To achieve the band fitting in Omnic, each file was individually opened, and a linear baseline correction was performed. The option to also perform a quadratic or cubic baseline were available, however we determined that this often removed small, relevant shoulder peaks within the spectra. The area between 1520 – 1385 cm^{-1} was enhanced and "Peak Resolve" was chosen from the tool bar. It was discovered to be important to maintain this selected area, as decreasing or increasing the magnitude of the X axis changed how the software located peaks. A gaussian fit was chosen at high sensitivity and the default FWHH was used. Any changes to the FWHH would be automatically corrected by the software upon fitting. The "Noise Target" of 2.75 was chosen empirically with the goal of ensuring the software could find all 4 desired peaks. A second linear baseline was chosen for consistency, but it was discovered to not have any effect on the spectral calculations since a baseline was already performed. Figure A1 shows the deconvolution of the 4 characteristic peaks.

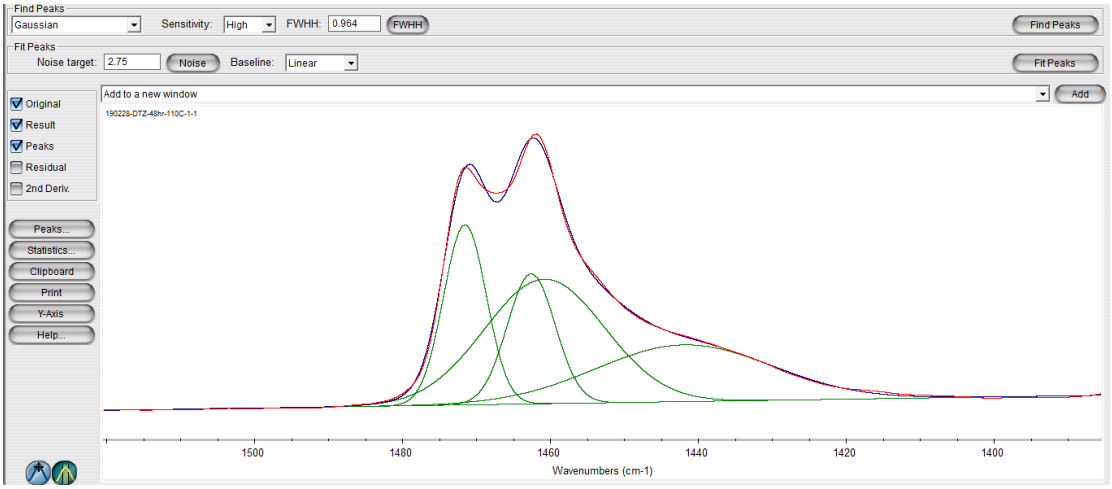

Figure A2: Spectra by Omnic "Peak Resolve" after selecting "Peak Fit". Notice the sharp crystalline singlet to the left, two overlapping amorphous peaks and broad shoulder to the right.

Selecting "Find Peaks" initiated the deconvolution process and in cases of a noisy spectra, more than 4 peaks were 'found' but then manually removed until the 4 characteristic peaks remain. 250 iterations were performed with a least-square fit parameter. This process is repeated several times until the peaks and fit parameter stop changing. The two amorphous peaks overlapped to a high degree, while the crystalline peak typically remained thinner and taller. The broad shoulder peak, an A_g resonance vibration of the lattice[87], was required to be included to ensure the 3 bands related to the crystallinity for converged properly but is not used for calculations. In heavily oxidized samples, a second smaller distinct shoulder peak appeared to the right of the broad peak. There has been no characterization of this peak either, but it was not removed as it helps maintain the integrity of the broad shoulder peak.

Thermal aging of polyethylene at 120°C was also performed to provide support for the studies done at 110°C. Figure A2 compares the calculated carbonyl index from both aging studies. An accelerated carbonyl growth is also seen in the 120°C, however occurring sooner than that of the 110°C aging. This is attributed to the increased thermal energy. Due to complete melting of many of the samples, timepoints of 264 & 336 hours were not taken.

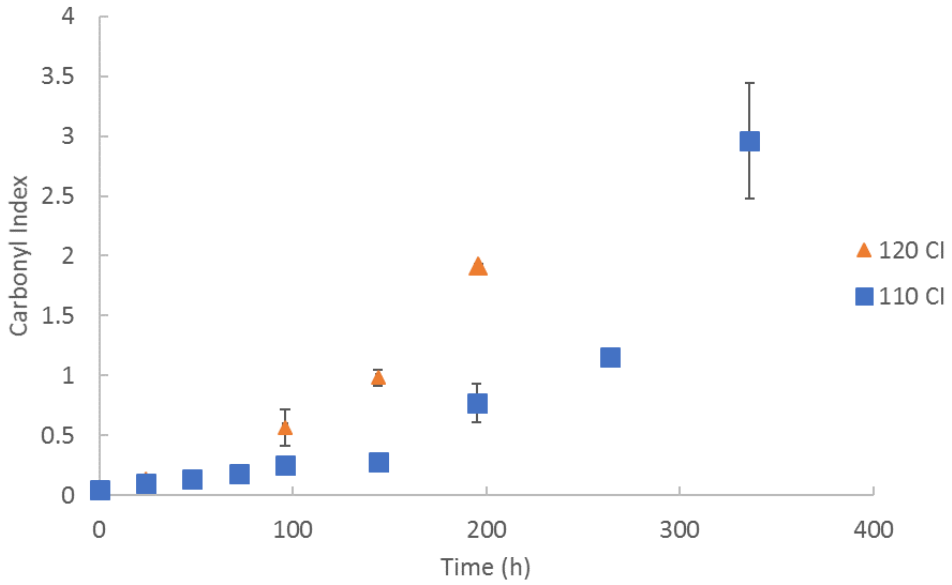

Figure A3: Comparison of the carbonyl content of polyethylene aged at 110°C and 120°C

The ATR-FTIR crystallinity method was also used to analyze the samples aged at 120°C, seen in Figure A3. The results reveal a net increase in crystallinity, however the annealing peak seen in the 110°C aging was not present. We hypothesize that significant melting of the polyethylene did not allow for the α-relaxation period, disrupting any crystalline structure present, however this cannot be confirmed by literature.

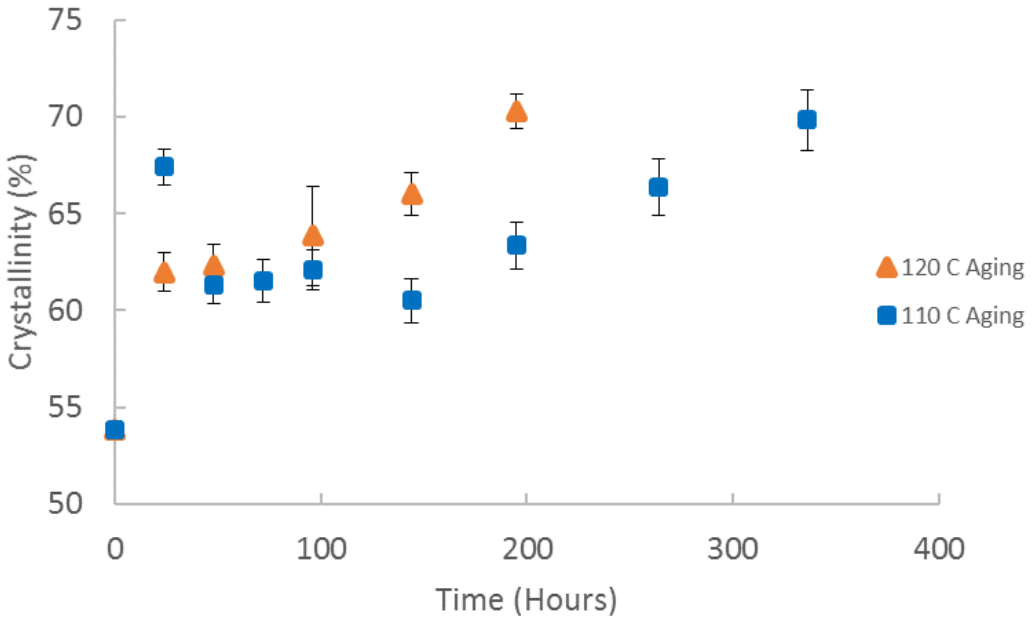

Figure A4: Comparison of the crystallinity of polyethylene aged at 110°C and 120°C

EIS measurements prior to the 110°C polyethylene aged for 55 days at 78°C was analyzed using EIS (Figure A4). The aged film was cut into several pieces which were placed in individual EIS cell setups. The MQMQ control sample showed no breakdown in impedance (no applied voltage). The samples run in an AuNP/MQ cell were subjected to both a +1 and -1 voltage. Both samples show no change in impedance. The samples run in an $HAuCl_4$/MQ cell were subjected to both a +1 and -1 voltage. Both samples showed a decrease in impedance. No further analysis was performed.

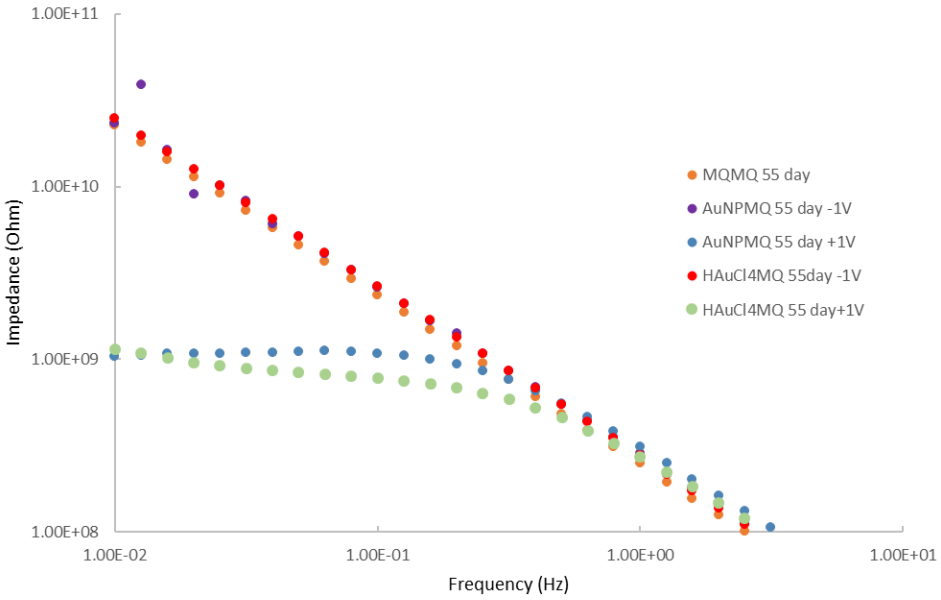

Figure A5: EIS results for 55 day aged polyethylene at 78°C.

Figure A6: EDS image of the AuNP facing (A) and MQ facing (B) sides of polyethylene aged for 336 hours, as well as the counter electrode (C). Note the large amount of charging on the surface, manifesting as lightening-like lines. Each spectral box indicates the area of analysis. Imaging at 25 kV.

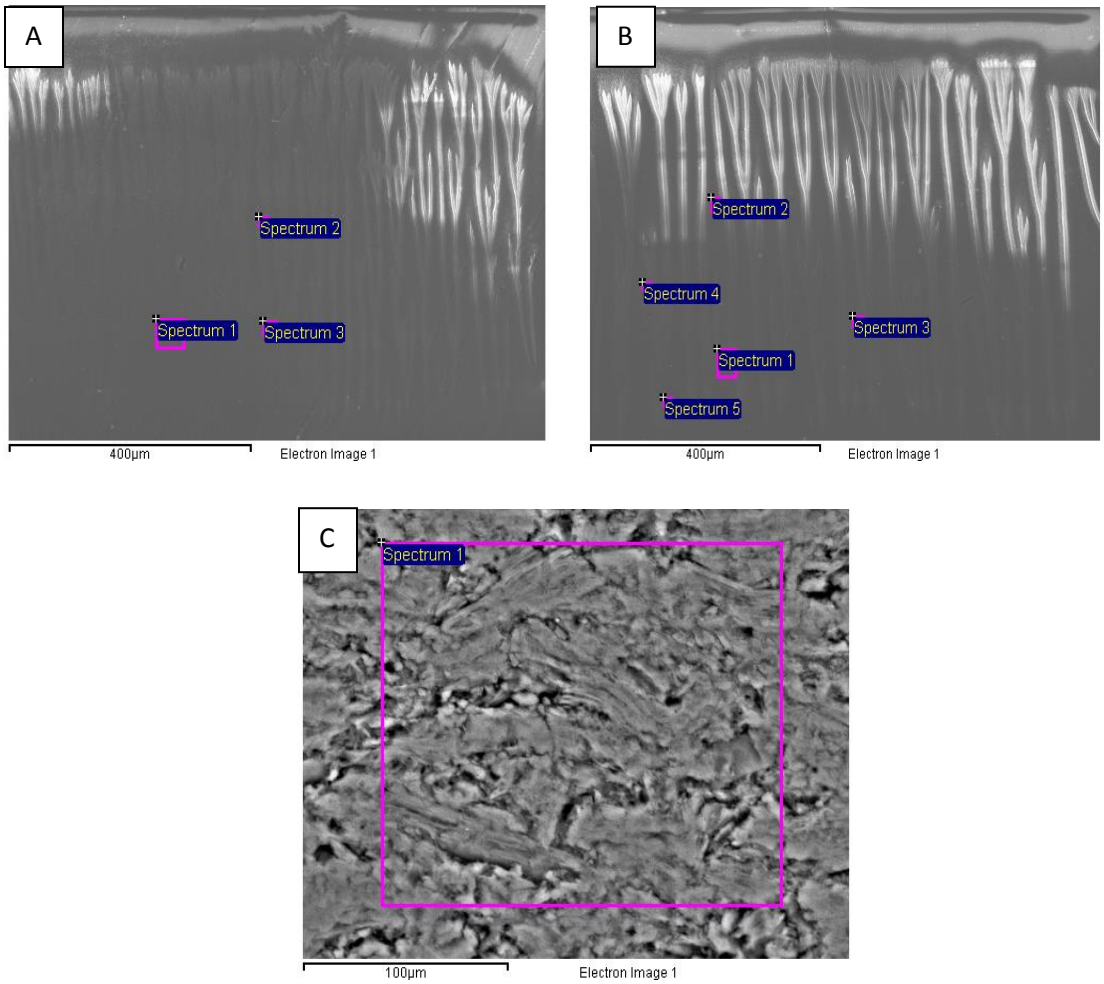
A
Spectrum 2
Spectrum 1
Spectrum 3
400µm
Electron Image 1
B
Spectrum 2
Spectrum 4
Spectrum 3
Spectrum 1
Spectrum 5
400µm
Electron Image 1
C
Spectrum 1
100µm
Electron Image 1

Figure A7: EDS image of the $HAuCl_4$ facing (A) and MQ facing (B) sides of polyethylene aged for 264 hours, as well as the counter electrode (C). Note the small increases in signal intensity on image X due to the presence of gold within the polymer surface. Charging is still seen. Imaging at 25 kV.